Seasonal variability of nitrous oxide concentrations and emissions in a temperate estuary

Gesa Schulz[1,2], Tina Sanders[2], Yoana G. Voynova[2], Hermann W. Bange[3], and Kirstin Dähnke[2]

[1]Institute of Geology, Center for Earth System Research and Sustainability (CEN), University Hamburg, Hamburg, 20146, Germany
[2]Institute of Carbon Cycles, Helmholtz Centre Hereon, Geesthacht, 21502, Germany
[3]Marine Biogeochemistry Research Division, GEOMAR Helmholtz Centre for Ocean Research Kiel, Kiel, 24105, Germany

Correspondence to: Gesa Schulz (Gesa.Schulz@hereon.de)

Abstract

Nitrous oxide (N_2O) is a greenhouse gas, with a global warming potential 298 times that of carbon dioxide. Estuaries can be sources of N_2O, but their emission estimates have significant uncertainties due to limited data availability and high spatiotemporal variability. We investigated the spatial and seasonal variability of dissolved N_2O and its emissions along the Elbe Estuary (Germany), a well-mixed temperate estuary with high nutrient loading from agriculture. During nine research cruises performed between 2017 and 2022, we measured dissolved N_2O concentrations, as well as dissolved nutrients and oxygen concentrations along the estuary and calculated N_2O saturations, flux densities and emissions. We found that the estuary was a year-round source of N_2O, with highest emissions in winter when dissolved inorganic nitrogen (DIN) loads and wind speeds are high. However, in spring and summer, N_2O saturations and emissions did not decrease alongside lower riverine nitrogen loads, suggesting that estuarine in-situ N_2O production is an important source of N_2O. We identified two hot-spots areas of N_2O production: the Port of Hamburg, a major port region, and the mesohaline estuary near the maximum turbidity zone (MTZ). N_2O production was fueled by decomposition of riverine organic matter in the Hamburg Port and by marine organic matter in the MTZ. A comparison with previous measurements in the Elbe Estuary revealed that N_2O saturation did not decrease alongside the decrease in DIN concentrations after a significant improvement of water quality in the 1990s that allowed for phytoplankton growth to reestablish in the river and estuary. The overarching control of phytoplankton growth on organic matter and, subsequently, on N_2O production, highlights the fact that eutrophication and elevated agricultural nutrient input can increase N_2O emissions in estuaries.

1 Introduction

Nitrous oxide (N_2O) is an important atmospheric trace gas that contributes to global warming and stratospheric ozone depletion (WMO, 2018; IPCC, 2021). Estuaries are important regions of nitrogen turnover (Middelburg and Nieuwenhuize, 2000; Crossland et al., 2005; Bouwman et al., 2013), and a potential source of N_2O (Bange, 2006; Barnes and Upstill-Goddard, 2011; Murray et al., 2015). Together with coastal wetlands, estuaries contribute between 0.17 and 0.95 Tg N_2O-N of the annual global budget of 16.9 Tg N_2O-N (Murray et al., 2015; Tian et al., 2020). N_2O emission estimates from estuaries are associated with significant uncertainties due to limited data availability and high spatiotemporal variability (e.g. Bange, 2006; Barnes and Upstill-Goddard, 2011; Maavara et al., 2019), presenting a big challenge for the global N_2O emission estimates.

Nitrification and denitrification are the most important N_2O production pathways in estuaries. Under oxic conditions, N_2O is produced as a side product during the first step of nitrification, the oxidation of ammonia to nitrite (e.g. Wrage et al., 2001; Barnes and Upstill-Goddard, 2011). At low oxygen (but not anoxic) conditions, nitrifier-denitrification may occur, during which nitrifiers reduce nitrite to N_2O (e.g. Wrage et al., 2001; Bange, 2008). Denitrification takes place under anoxic conditions and mostly acts as a source of N_2O, but can also reduce N_2O to N_2 (e.g. Knowles, 1982; Bange, 2008). In estuaries, denitrification can occur in anoxic sediments, the anoxic water column or anoxic microsites of particles, whereas nitrification and nitrifier-denitrification take place in the oxygenated water column (Beaulieu et al., 2010; Murray et al., 2015; Ji et al., 2018; Tang et al., 2022).

In estuaries, the most important factors controlling N_2O emissions are considered to be oxygen availability and dissolved inorganic nitrogen loads (Murray et al., 2015). Since N_2O measurements in estuaries are scarce, global N_2O emissions can be estimated by using emission factors and considering dissolved inorganic nitrogen (DIN) or total nitrogen (TN) loads, where it is assumed that higher nitrogen loads lead to higher N_2O emissions (Kroeze et al., 2005, 2010; Ivens et al., 2011; Hu et al., 2016). However, several studies instead reported no obvious relationship between nitrogen concentrations and N_2O emissions (Borges et al., 2015; Marzadri et al., 2017; Wells et al., 2018), highlighting the need to understand the causes for variability in the relationship between nitrogen loads and N_2O emissions (Wells et al., 2018).

The Elbe Estuary is a heavily managed estuary with high agricultural nitrogen inputs that hosts the third largest port in Europe (e.g. Radach and Pätsch, 2007; Bergemann and Gaumert, 2008; Pätsch et al., 2010; Quiel et al., 2011). It has been identified as a N_2O source, with a hotspot of N_2O production in the Port of Hamburg (Hanke and Knauth, 1990; Brase et al., 2017). We aimed to investigate drivers for N_2O emissions along the estuary, specifically the N_2O and DIN ratio (N_2O:DIN). To do so, we (1) looked for potential long-term changes in N_2O saturations, (2) investigated potential production hotspots, as well as the spatial and temporal distribution of N_2O saturations, and (3) used the N_2O:DIN ratio for a comparison with other estuaries.

2   Methods

2.1   Study site

The Elbe River stretches over 1094 km from the Giant Mountains (Czech Republic) to the North Sea (Cuxhaven, Germany). The catchment of the Elbe River is 140 268 km² (Boehlich and Strotmann, 2019), with 74 % urban and agricultural land-use (Johannsen et al., 2008).The Elbe is the second largest German river discharging into the North Sea, as well as the largest source of dissolved nitrogen for the German Bright, which is heavily affected by eutrophication (van Beusekom et al., 2019).

The Elbe Estuary is a well-mixed temperate estuary, which begins at stream kilometer 586 at a weir in Geesthacht and stretches through the Port of Hamburg, entering the North Sea near Cuxhaven at stream kilometer 727 (Fig. 1). Estuaries are commonly structured along their salinity gradient into an oligohaline (salinity: 0.5 – 5.0), a mesohaline (salinity: 5.0 – 18.0) and a polyhaline (salinity > 18.0) region (US EPA, 2006). The Elbe Estuary has a length of 142 km (Boehlich and Strotmann, 2019) and a mean annual discharge of 712 m³ s^{-1} (measured at gauge Neu Darchau at stream kilometer 536; HPA and Freie und Hansestadt Hamburg, 2017). The average water residence time is ~32 days, ranging from ~72 days during times of low discharge (300 m³ s^{-1}) to ~10 days during times of high discharge (2000 m³ s^{-1}; Boehlich and Strotmann, 2008). The Elbe Estuary has an annual nitrogen load of 84 Gg-N (FGG Elbe, 2018), and point sources along the estuary provide only a small part of the total

78 nitrogen input (Hofmann et al., 2005; IKSE, 2018). Oxygen concentrations in the Elbe Estuary vary seasonally,
79 with oxygen depletion during the summer months and oxygen minimum zones regularly experiencing
80 concentrations below 94 µmol O_2 L^{-1} (Schroeder, 1997; Gaumert and Bergemann, 2007; Schöl et al., 2014).
81 The Elbe Estuary is dredged year-round to maintain a water depth of 15 – 20 m and to grant access for large
82 container ships to the Port of Hamburg (Boehlich and Strotmann, 2019; Hein et al., 2021). Construction work for
83 further deepening of the fairway was carried out during our study period, from 2019 to early 2022. Upstream of
84 the Port of Hamburg water depth is less than 10 m (Hein et al., 2021).

85
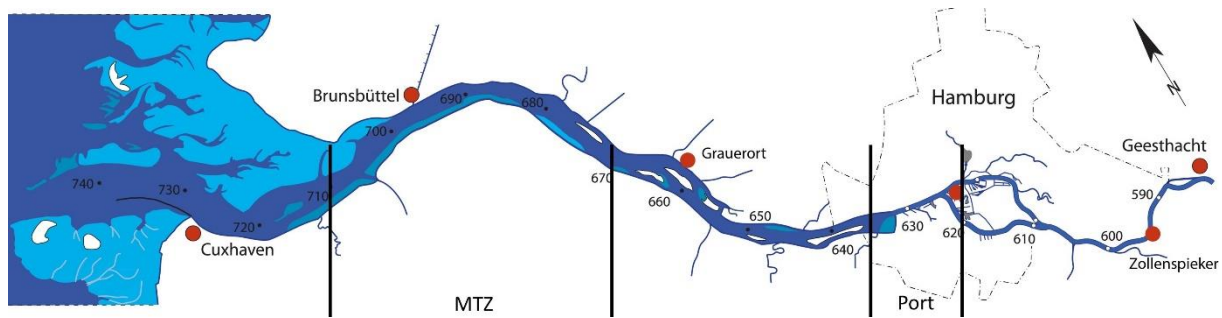
87 **Figure 1: Map of the Elbe Estuary sampled during our research cruises with stream kilometers (graphic courtesy of**
88 **FGG Elbe, modified after Amann et al. 2012)). The light blue color indicates Wadden Sea areas that are exposed at low**
89 **tide. The vertical black lines indicate the Hamburg Port region and a typical position for the maximum turbidity zone**
90 **(MTZ, Bergemann, 2004).**

91 **2.2   Transect sampling and measurements**

92 We performed nine sampling campaigns along the estuary with the research vessel *Ludwig Prandtl* (Table 1). Most
93 cruises took place during spring and summer, with water temperatures > 10 °C (May to September). Two cruises
94 were conducted during winter (early March, water temperature < 6 °C; Table 1). Transects started in the German
95 Bight, and continued along the salinity gradient, through the Port of Hamburg to Oortkaten (stream kilometer 609).
96 To ensure comparable current and mixing conditions, transect sampling was always done after high-tide, with the
97 ship travelling upstream against the tide. For comparison to previous measurements, we included summer data
98 from a previous study in 2015 (Brase et al., 2017).

99 **Table 1: Campaign dates with the sampled Elbe Estuary sections shown via stream kilometers, average discharge**
100 **during each cruise measured at the Neu Darchau gauging station, averages and standard deviations for water**
101 **temperature, wind speed at 10 m height, dissolved inorganic nitrogen (DIN) concentrations for each campaign.**

Campaign Dates	Stream kilometers (km)	Water temperature (°C)	Wind speed 10 m (m s^{-1})	Average discharge (m³ s^{-1})	Average DIN concentrations (µmol L^{-1})
28.-29.04.2015	627 – 741	12.3 ± 1.0	7.4 ± 2.3	595	191.0 ± 45.0
02.-04.06.2015	609 – 739	17.4 ± 1.7	5.0 ± 1.3	276	105.9 ± 36.2
01.-02.08.2017	621 – 749	20.9 ± 0.7	3.6 ± 1.5	607	79.2 + 30.2
04.-05.06.2019	610 – 750	18.7 ± 2.2	4.0 ± 1.7	423	108.3 ± 35.9
30.07.-01.08.2019	609 – 752	22.6 ± 1.0	4.2 ± 1.4	171	60.8 ± 38.6
19.-20.06.2020	609 – 747	19.8 ± 1.4	5.8 ± 1.2	331	74.6 ± 33.8
09.-11.09.2020	607 – 745	18.9 ± 0.6	5.9 ± 2.8	305	93.1 ± 32.7
10.-12.03.2021	609 – 748	5.4 ± 0.5	9.3 ± 2.6	862	324.4 ± 83.8
04.-05.05.2021	610 – 751	10.5 ± 0.8	11.0 ± 3.1	411	85.7 ± 36.6
27.-28.07.2021	621 – 751	22.2 ± 0.7	5.2 ± 1.3	721	139.8 ± 58.4
01.-02.03.2022	610 – 752	5.6 ± 0.2	2.9 ± 1.0	1282	238.0 ± 74.7

102 An onboard membrane pump continuously provided water at 1.2 m depth to an on-line in-situ FerryBox system
103 and to an equilibrator used for the measurements of N_2O dry mole fraction (Section 2.4). The FerryBox system
104 continuously measured water temperature, salinity, oxygen concentrations, pH and turbidity. We corrected the
105 salinity corrected optode measurements using comparisons to Winkler titrations of discrete samples. See Table S1
106 for further details.

107 Discrete water samples (30-40 samples for each cruise) were collected every 20 min from a bypass of the FerryBox
108 system. For nutrient analysis, water samples were filtered immediately through combusted, pre-weighted GF/F
109 Filters (4 h, 450 °C), and were frozen in acid washed PE-bottles until analysis. The filters were also stored frozen
110 (-20 °C) and subsequently analyzed for suspended particulate matter (SPM), particulate nitrogen (PN), total
111 particulate carbon (PC) and C/N ratios (Fig. S1).

112 **2.3   Nutrient measurements**

113 Filtered water samples were measured in triplicates with a continuous flow auto analyzer (AA3, SEAL Analytics)
114 using standard colorimetric and fluorometric methods (Hansen and Koroleff, 1999) for dissolved nitrate (NO_3^-),
115 nitrite (NO_2^-) and ammonium (NH_4^+) concentrations. Detection limits were 0.05 µmol L^{-1}, 0.05 µmol L^{-1}, and
116 0.07 µmol L^{-1} for nitrate, nitrite and ammonium, respectively.

117 **2.4   Equilibrator based N_2O measurements and calculations**

118 Equilibrated dry mole fractions of N_2O were measured by an N_2O analyzer based on off-axis integrated cavity
119 output (OA-ICOS) absorption spectroscopy (Model 914-0022, Los Gatos Res. Inc., San Jose, CA, USA), which
120 was coupled with a seawater/gas equilibrator using off-axis cavity output spectroscopy. Brase et al. (2017)
121 described the set-up and instrument precision in detail. Twice a day, two standard gas mixtures of N_2O in synthetic
122 air (500.5 ppb ± 5 % and 321.2 ppb ± 3 %) were analyzed to validate our measurements. No drift was detected
123 during our cruises.

4

We calculated the dissolved N_2O concentrations in water with the Bunsen solubility function of Weiss and Price (1980), using 1 min averages of the measured N_2O dry mole fraction (ppb). Temperature differences between the sample inlet and the equilibrator were taken into account for the calculation of the final N_2O concentrations Rhee et al. (2009). N_2O saturation was calculated based on N_2O concentrations in water (N_2O_{cw}) and the atmospheric equilibration concentrations (N_2O_{eq}; Eq. 1). Atmospheric N_2O dry mole fractions were measured before and after each transect cruises using an air duct from the deck of the research vessel.

$$s = 100 \times \frac{N_2O_{cw}}{N_2O_{eq}} \tag{1}$$

The gas transfer coefficients (k) were determined based on Borges et al. (2004, Eq. 3), Nightingale et al. (2000), Wanninkhof (1992) and Clark et al. (1995), using the Schmidt number (Sc) and wind speeds (u_{10}) measured at 10 m height (Eq. 2). The Schmidt number was calculated as ratio of the kinematic viscosity in water (Siedler and Peters, 1986) to the N_2O diffusivity in water (Rhee, 2000). Cruise wind speeds (Table 1) varied significantly from average annual wind speeds of the two federal states, in which the Elbe Estuary is located (4.7 m s^{-1}, Schleswig-Holstein u. Hamburg: Mittlere Windgeschwindigkeit (1986-2015)* | Norddeutscher Klimamonitor, 2023), and also compared to seasonal average wind speeds determined for the stations Cuxhaven and Hamburg (Rosenhagen et al., 2011). Thus, to estimate uncertainties due to varying wind conditions during our cruises, we used 1) the *in-situ* wind speeds measured on board the *R/V Ludwig Prandtl* at 10 m height by a MaxiMet GMX600 (Gill Instruments Limited, Hampshire, UK), 2) the average annual wind speed (Schleswig-Holstein u. Hamburg: Mittlere Windgeschwindigkeit (1986-2015)* | Norddeutscher Klimamonitor, 2023), and 3) the seasonally averaged wind speeds (Rosenhagen et al., 2011). The flux densities in the main text were calculated using Eq. 3 and the wind speeds measured on board the vessel. Results of the other calculations are listed in the supplementary material (Table S2).

$$k = 0.24 \times (4.045 + 2.58u_{10}) \times \left(\frac{Sc}{600}\right)^{-0.5} \tag{2}$$

$$f = k \times (N_2O_{cw} - N_2O_{air}) \tag{3}$$

To estimate N_2O emissions, we separated the Elbe Estuary into five regions: limnic (stream kilometer 585 to 615), Port of Hamburg (stream kilometer 615 to 632), oligohaline (stream kilometer 632 to 704), mesohaline (stream kilometer 704 – 727) and polyhaline (stream kilometer 727 to 750), see Table S3. Respective areas were provided by the German Federal Waterways Engineering and Research Institute (BAW, pers. Comm., Oritz, 2023) and Geerts et al. (2012). In order to account for seasonality, cruises were defined as: winter (March), spring (April and May), summer (June and July) and late summer/autumn (August and September). We then calculated daily N_2O emissions per section and season. For upscaling, we used the calculated monthly emissions to estimate annual emissions (winter: November to March, spring: April to May, summer: June to July and late summer/autumn: August to October). To address uncertainties, we calculated N_2O emissions based on different parametrizations and wind speeds as described above.

2.5 Excess N_2O and apparent oxygen utilization

The correlation between excess N_2O (N_2O_{xs}) and apparent oxygen utilization (AOU) can provide insights into N_2O production (Nevison et al., 2003; Walter et al., 2004). We calculated N_2O_{xs} as the difference between the N_2O concentration in water and the theoretical equilibrium concentration (N_2O_{eq}) (Eq. 4). AOU was determined using

158   Eq. 5, where O_2 is the measured dissolved oxygen concentration, and $O_2^{'}$ is the theoretical equilibrium

159   concentration between water and atmosphere calculated according to Weiss (1970).

$$N_2O_{xs} = N_2O_{cw} - N_2O_{eq} \qquad (4)$$

$$AOU = O_2' - O_2 \qquad (5)$$

160   A linear relationship between AOU and N_2O_{xs} is usually an indicator for N_2O production from nitrification

161   (Nevison et al., 2003; Walter et al., 2004).

162   **2.6   Statistical analysis**

163   All statistical analyses were done using R packages. The packages ggpubr v.0.6.0 (Kassambara, 2023) and stats

164   v.4.0.2 (The R Stats Package, Version 4.0.2, 2021) were used to calculate Pearson correlations (*R*) and *p*-values.

165   **3   Results**

166   **3.1   Hydrographic properties and DIN distribution**

167   Discharge ranged between 171 m³ s⁻¹ and 1282 m³ s⁻¹ during our cruises (ZDM, 2022), with higher discharge in

168   winter and lower discharge in summer (Table 1). Average water temperature over the entire estuary ranged from

169   5.4 ± 0.5 °C in March 2021 to 22.6 ± 1.0 °C in August 2017 (Table 1). For further evaluation, March 2021 and

170   2022 cruises were regarded as winter cruises (water temperature < 6°C), whereas all cruises with higher water

171   temperature were jointly regarded as spring and summer conditions.

172   Nitrate was the major form of dissolved inorganic nitrogen (DIN) during all cruises. In winter, high nitrogen

173   concentrations entered the estuary from the river. Towards summer, the riverine input of nitrate (stream kilometer

174   < 620) decreased, but along the estuary nitrate concentrations increased up to ~stream kilometer 700, then

175   decreased towards the North Sea. Nitrate concentrations were highest during both March cruises with averages of

176   319.0 ± 85.7 µmol L⁻¹ and 230.9 ± 76.2 µmol L⁻¹ in 2021 and 2022, respectively. During summer, nitrate

177   concentrations were lower, with averages between 151.0 ± 58.1 µmol L⁻¹ in May 2021 and 63.3 ± 38.8 µmol L⁻¹

178   in July 2019 (Fig. 2a and b).

179   Nitrite and ammonium concentrations were usually low (< 1 µmol L⁻¹) throughout the Elbe Estuary, but peaked

180   in the Hamburg Port region and around stream kilometer 720 (Fig. 2c and 2e). We measured pronounced variations

181   in nitrite concentrations during most of our cruises, ranging from > 6.0 µmol L⁻¹ (July 2019) to concentrations

182   below the detection limit (Fig. 2c and d). The highest ammonium concentration was measured in March 2021 at

183   23.5 µmol L⁻¹ (Fig. 2e and f).
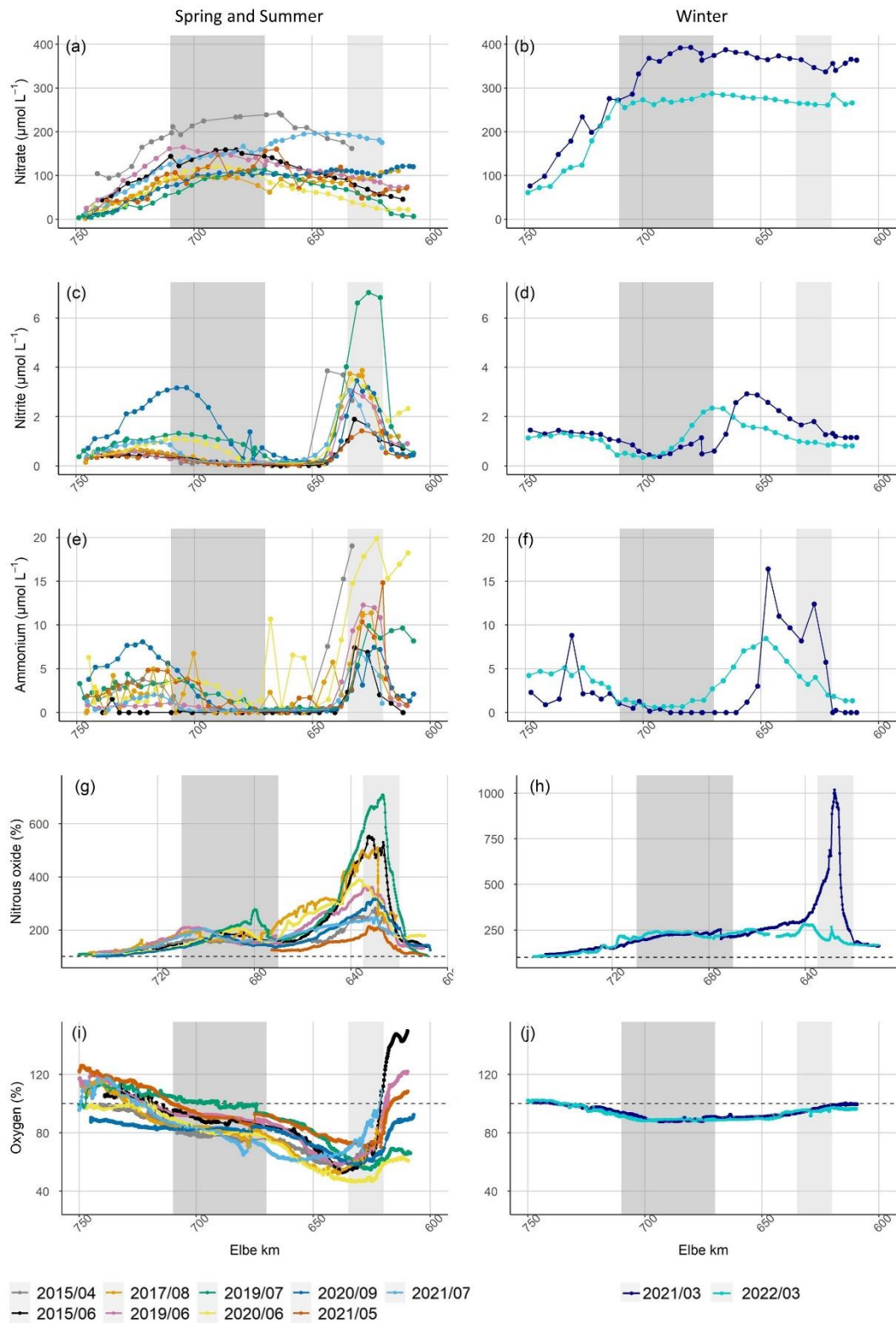
Figure 2: Nitrate concentration along the Elbe Estuary (a) in spring/summer, (b) in winter. Nitrite concentration along the Elbe Estuary (c) in spring/summer and (d) in winter. Ammonium concentration along the Elbe Estuary (e) in spring/summer and (f) in winter. N₂O in % saturation along the Elbe Estuary (g) in spring/summer, (h) in winter. Dissolved oxygen in % saturation along the Elbe Estuary (i) in spring/summer and (j) in winter. All variables are plotted against Elbe stream kilometers (Elbe km). Light grey shading denotes the Hamburg Port region, dark grey shading the typical position of the maximum turbidity zone (MTZ, Bergemann, 2004). Note the difference in Y-axis scales for the plots of (g) and (h). The dashed black lines in (g) and (h), as well (i) and (j) indicate saturation of 100 % for nitrous oxide and dissolved oxygen, respectively.

7

3.2 Atmospheric N$_2$O and N$_2$O saturation

The average atmospheric N$_2$O dry mole fractions ranged from 325 ppb in June 2015 to 336 ppb in July 2022 (Table 2). The differences between our measurements and the mean monthly N$_2$O mole fraction measured at the Mace Head atmospheric monitoring station (Ireland; Dlugokencky et al., 2022) were always less than 1.5 %, indicating a good agreement with the monitoring data.

During all cruises, the Elbe Estuary was supersaturated in N$_2$O in the freshwater region (Fig. 2g, h). The average N$_2$O saturation over the entire transect ranged between 146 % and 243 % with an overall average of 197 % for all cruises. Highest N$_2$O occurred in the Hamburg Port region in spring and summer with an average N$_2$O peak of 402 % saturation and a maximum supersaturation of 710 % in July 2019. The distributions of N$_2$O during winter cruises were significantly different: In March 2022, highest N$_2$O (280 % saturation) occurred at stream kilometer 640. In contrast, in March 2021, we found an extraordinarily high peak with a saturation of 1018 % at stream kilometer 627. Between stream kilometer 680 and 720, a supersaturation of up to 277 % occurred in spring and summer. Further towards the North Sea, N$_2$O decreased, approaching equilibrium with the atmosphere.

3.3 N$_2$O flux densities and N$_2$O emissions

For N$_2$O flux densities, we present calculated values after Borges et al. (2004, Table 2), but also include results using other parametrizations in Table S2 and Fig. S2. The N$_2$O flux densities were usually highest in the Hamburg Port area, with an average of 95.0 ± 97.9 µmol m^{-2} d^{-1} and lowest towards the North Sea, with an average of 3.9 ± 3.0 µmol m^{-1} d^{-1} (Elbe stream kilometers > 735). The average N$_2$O flux density of all cruises was 39.9 ± 46.9 µmol m^{-2} d^{-1} (calculated with *in-situ* wind speeds measured during the cruises).

Table 2: Calculated average N$_2$O saturation, sea-to-air fluxes calculated following Borges et al. (2004) and atmospheric N$_2$O dry mole fractions during our cruises in the Elbe Estuary

Campaign Dates	Average saturation (%)	N$_2$O Flux densities (µmol m^{-2} d^{-1})			Average atmospheric dry mole fraction (ppb)
		In-situ wind	Annual wind	Seasonal wind	
28.-29.04.15	160.8 ± 37.9	33.1 ± 21.0	23.1 ± 14.7	25.4 ± 16.1	331 ± 0.5
02.-04.06.15	203.8 ± 112.7	39.0 ± 42.7	37.2 ± 40.7	37.8 ± 41.4	325 ± 0.8
01.-02.08.17	221.0 ± 106.5	35.6 ± 31.8	43.2 ± 38.5	44.1 ± 39.3	331 ± 1.2
04.-05.06.19	192.6 ± 66.0	29.7 ± 21.5	33.5 ± 24.2	34.0 ± 24.6	332 ± 0.2
30.07.-01.08.19	232.5 ± 155.3	42.0 ± 50.1	45.7 ± 54.5	47.4 ± 56.4	327 ± 1.0
19.-20.06.20	193.9 ± 74.1	39.2 ± 31.6	33.3 ± 26.9	33.9 ± 27.3	330 ± 0.6
09.-11.09.20	160.5 ± 53.6	26.0 ± 23.5	21.8 ± 19.7	24.5 ± 22.1	331 ± 0.7
10.-12.03.21	242.5 ± 141.6	100.7 ± 101.2	58.1 ± 58.4	71.0 ± 71.4	331 ± 1.3
04.-05.05.21	145.6 ± 28.8	35.6 ± 22.5	17.8 ± 11.2	18.5 ± 11.7	331 ± 0.8
27.-28.07.21	172.6 ± 37.2	28.0 ± 14.6	25.9 ± 13.6	26.9 ± 14.1	334 ± 3.8
01.-02.03.22	196.5 ± 47.0	27.8 ± 13.9	39.0 ± 19.5	47.7 ± 23.8	333 ± 0.7

N$_2$O emission estimates varied significantly depending on the used parametrization and wind speeds. Note that we calculated emissions twice: 1) including (w 03/2021) and 2) deliberately excluding (w/o 03/2021) the N$_2$O peak saturation measured in the Port of Hamburg in March 2021, using linearly interpolated concentrations, respectively. Highest emissions were calculated following methods by Borges et al. (2004) and using *in-situ* wind

8

219 speeds, resulting in emissions of 0.25 ± 0.16 Gg-N_2O yr^{-1} and 0.23 ± 0.12 Gg-N_2O yr^{-1} with and without the N_2O

220 peak in March 2021, respectively. Lowest emissions of 0.08 Gg-N_2O yr^{-1} arose with parametrization of Nightingale

221 et al. (2000) and Wanninkhof (1992), and using annual wind speeds (Table 3).

222 **Table 3: Annual N_2O emission estimates in Gg-N_2O yr^{-1} calculated with different parametrizations and wind speeds**

| | | Emissions in Gg-N_2O yr^{-1} | | | |
		Borges et al. (2004)	Nightingale et al. (2000)	Wanninkhof (1992)	Clark et al. (1995)
w 03/2021	In-situ wind	0.25 ± 0.16	0.14 ± 0.12	0.17 ± 0.15	0.16 ± 0.12
	Annual wind	0.21 ± 0.11	0.08 ± 0.04	0.09 ± 0.05	0.09 ± 0.05
	Seasonal wind	0.24 ± 0.12	0.11 ± 0.06	0.13 ± 0.06	0.12 ± 0.06
w/o 03/2021	In-situ wind	0.23 ± 0.12	0.13 ± 0.09	0.15 ± 0.11	0.14 ± 0.09
	Annual wind	0.20 ± 0.08	0.08 ± 0.03	0.08 ± 0.03	0.09 ± 0.04
	Seasonal wind	0.22 ± 0.09	0.11 ± 0.04	0.12 ± 0.04	0.12 ± 0.04

223 **3.4 Dissolved oxygen saturation**

224 Average oxygen varied between 76 and 95 in % saturation with an oxygen minimum in the Hamburg Port area.

225 Winter cruises varied little, with oxygen remaining relatively constant along the estuary (> 88 % saturation).

226 During most spring and summer cruises, water from the river coming into the estuary was supersaturated in oxygen

227 (> 100 % saturation). In the Hamburg Port region, oxygen saturation generally decreased. Lowest values occurred

228 in June 2020 with 47 % saturation. The along-estuary oxygen minimum in summer months (June to August) was

229 always below 61 % saturation. In spring and summer, oxygen increased towards the North Sea and reached

230 100 % saturation (Fig. 2i and j).

231 Plots of excess N_2O (N_2O_{xs}) and apparent oxygen utilization (AOU) revealed excess N_2O along the entire estuary

232 (Fig. 3). During all cruises, elevated riverine N_2O_{xs} entered the estuary (stream kilometer < 620). A linear positive

233 relationship between N_2O_{xs} and AOU suggested nitrification as main production pathway in large sections of the

234 estuary (Nevison et al., 2003; Walter et al., 2004). However, in summer, a change of slope in the Port of Hamburg

235 as well as in the mesohaline section of the estuary suggested either increased in-situ N_2O production or external

236 N_2O input. In winter, we found an increasing slope in the Hamburg Port region and in the oligohaline part of the

237 Elbe Estuary (Fig. 3h, k).
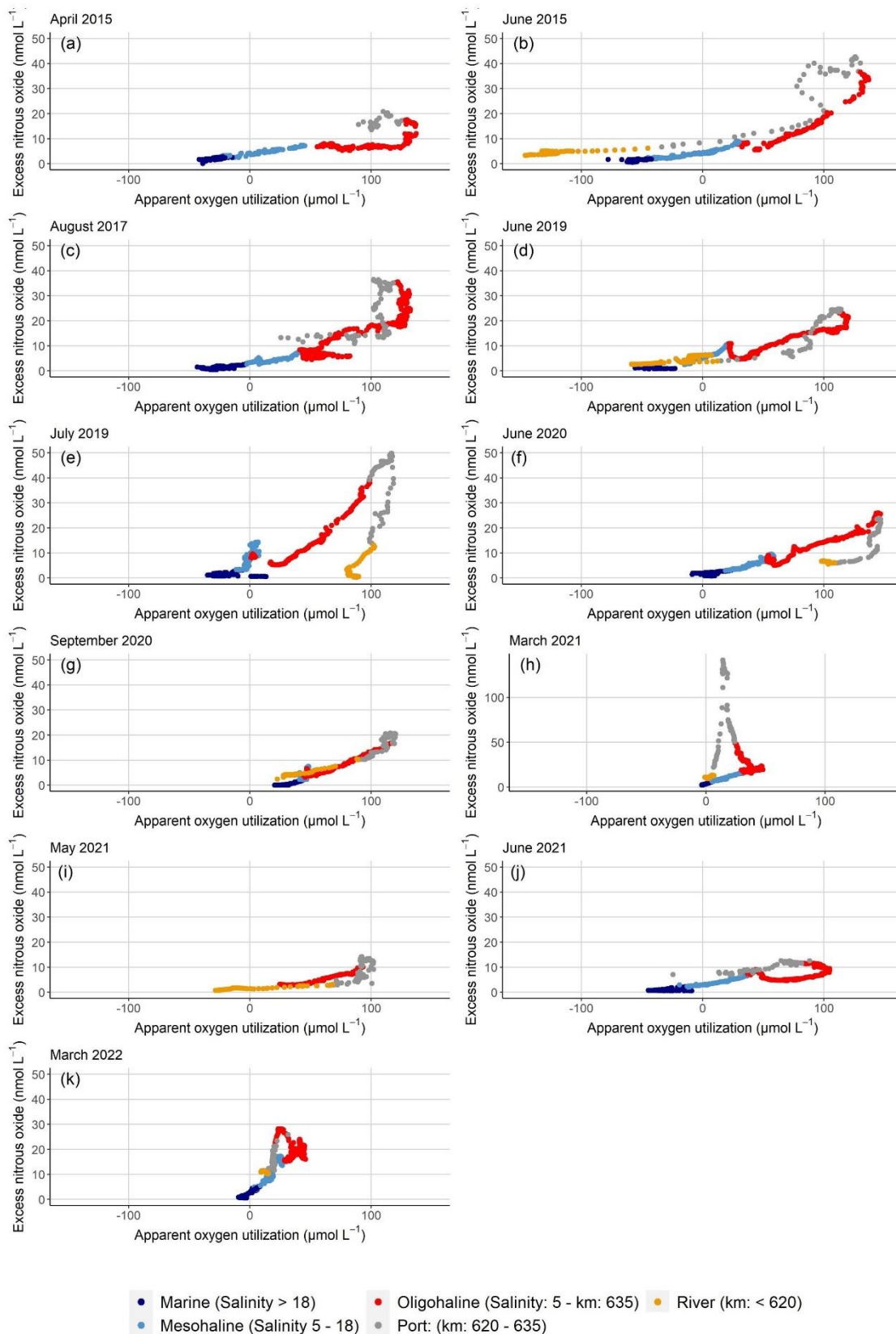
Figure 3: Plots of N_2O_{xs} vs AOU for (a) April 2015, (b) June 2015, (c) August 2017, (d) June 2019, (e) July 2019, (f) June 2020, (g) September 2020, (h) March 2021, (i) May 2021, (j) June 2021 and (k) March 2022. The values are colored to distinguish between different regions of the estuary. Y-axis scale differ for Fig. 3h.

3.5 Statistical analysis

We performed statistical analyses to identify potential N_2O production pathways and controlling factors. Table 4 summarizes the results for the entire data set with further separation into spring and summer cruises (sp/su), as well as separation according to the presence of a salinity gradient (salinity > 1) or of freshwater regions (salinity < 1). Furthermore, we performed corresponding analysis to assess the significance of correlations between for average values of different parameters for each cruise (Table 5). N_2O saturation showed significant negative correlation with oxygen (Table 4) as well as a consistent negative correlation with pH (Table 4 and 5). Furthermore, nitrite concentrations positively correlated with N_2O saturation in the freshwater section of the estuary (Table 4 and 5).

Table 4: Pearson correlation coefficients (R) for N_2O saturation (%) with temperature (T in °C), pH value, oxygen (O_2 in % saturation), ammonium concentrations (NH_4^+ in µmol L^{-1}), nitrite concentrations (NO_2^- in µmol L^{-1}), nitrate concentrations (NO_3^- in µmol L^{-1}), SPM concentrations (SPM in mg L^{-1}), C/N values, particulate carbon fraction (PC in %) and particulate nitrogen fraction (PN in %) for the entire data set, spring and summer cruises (sp/su), data with salinity > 1, spring and summer cruises with salinity > 1, data with salinity < 1 and spring and summer cruises with salinity < 1. The significance is shown as ** for p-value < 0.001, * for p-values < 0.01 and + for p-values < 0.05.

N_2O saturation %	T °C	pH	O_2 %	NH_4^+ µM	NO_2^- µM	NO_3^- µM	SPM mg	C/N	PC %	PN %
Entire data	0.06	-0.47**	-0.56**	0.27**	0.48**	0.23	0.10	0.60	-0.05	-0.13+
sp/su	0.33*	-0.59**	-0.65**	0.23**	0.53**	0.09	0.02	0.24**	-0.09	-0.13+
Sal>1	0.03	-0.40**	-0.53**	-0.32**	-0.05	0.71**	0.32**	0.11*	-0.24	-0.39**
Sal<1,	0.01	-0.41**	-0.42**	0.28**	0.51**	-0.00	-0.08	0.15	-0.25*	-0.24*
Sal>1, sp/su	-0.10	-0.21+	-0.52**	-0.28**	0.01	0.62**	0.02	0.39**	-0.31**	-0.41**
Sal<1, sp/su	0.30**	-0.60**	-0.57**	0.21+	0.58**	-0.23*	-0.16˙	0.11	-0.30*	-0.27*

Table 5: Pearson correlation coefficients (R) for average N_2O saturation (%) with average discharge (Q in m³ s^{-1}) temperature (T in °C), pH value, oxygen (O_2 in % saturation), ammonium concentrations (NH_4^+ in µmol L^{-1}), nitrite concentrations (NO_2^- in µmol L^{-1}), nitrate concentrations (NO_3^- in µmol L^{-1}), SPM concentrations (SPM in mg L^{-1}), C/N values, particulate carbon fraction (PC in %) and particulate nitrogen fraction (PN in %) for the entire data set, spring and summer cruises (sp/su), data with salinity > 1, spring and summer cruises with salinity > 1, data with salinity < 1 and spring and summer cruises with salinity < 1. The significance is shown as ** for p-value < 0.001, * for p-values < 0.01 and + for p-values < 0.05.

N_2O saturation %	Q m³s⁻¹	T °C	pH	O_2 %	NH_4^+ µM	NO_2^- µM	NO_3^- µM	SPM mg	C/N	PC %	PN %
Entire data	0.13	0.06	-0.65	-0.39	0.02	0.48	0.27	-0.31	0.53	0.12	-0.16
sp/su	-0.26	0.76+	-0.82+	-0.32	0.01	0.35	-0.40	-0.92*	0.15	0.18	0.31
Sal>1	-0.07	-0.14	-0.38	-0.43	-0.18	0.23	0.52	-0.19	0.46	-0.18	-0.38
Sal<1,	-0.21	0.29	-0.59	-0.39	0.26	0.76*	-0.11	-0.57	0.12	0.61	0.47
Sal>1, sp/su	-0.07	-0.70+	-0.41	-0.26	-0.42	0.03	0.05	-0.81+	-0.04	-0.10	0.14
Sal<1, sp/su	-0.48	0.72+	-0.80	-0.46	0.29	0.77+	-0.58	-0.87+	-0.17	0.69	0.67

4   Discussion

### 4.1 N_2O saturation and flux densities of the Elbe Estuary

The average N_2O saturation and flux density were 197 % and 39.9 ± 46.9 µmol m^{-2} d^{-1}, respectively. The N_2O flux densities from the Elbe Estuary were in the mid-range of flux densities of other European estuaries ranging from 2.9 µmol m^{-2} d^{-1} to 96.5 µmol m^{-2} d^{-1} (Garnier et al., 2006; Gonçalves et al., 2010; Murray et al., 2015) and average N_2O saturations fitted to values determined by Reading et al. (2020) for highly modified urban systems. The relationship of N_2O_{xs} and AOU (Fig. 3), with changing slopes in the Port of Hamburg and mesohaline estuary, was determined by either initial riverine N_2O production, or in-situ production along the estuary. During spring and summer, we found increasing N_2O concentrations in the Hamburg Port region (see also Brase et al. (2017)), and in the salinity gradient (stream kilometer 680 – 700, salinity ~5). Both N_2O peaks varied in magnitude and spatial extension, suggesting in-situ biological production (Fig. 2g). This matches earlier research linking estuarine N_2O fluxes to in-situ generation (e.g. Bange, 2006; Barnes and Upstill-Goddard, 2011; Murray et al., 2015).

Previous measurements of N_2O saturation and flux densities in the Elbe Estuary between the 1980s and 2015 (Hanke and Knauth, 1990; Barnes and Upstill-Goddard, 2011; Brase et al., 2017) showed a significant reduction of N_2O saturation due to the reduced riverine nutrient load and higher dissolved oxygen concentrations (Brase et al., 2017). However, since the BIOGEST study in 1997 (Barnes and Upstill-Goddard, 2011), N_2O remained relatively stable at ~ 200 % saturation despite a concurrent decrease in TN concentration from ~400 µmol L^{-1} to around 200 µmol L^{-1} (Fig. S3; Hanke and Knauth, 1990; Barnes and Upstill-Goddard, 2011; Brase et al., 2017; Das Fachinfomrationssystem (FIS) der FGG Elbe, 2022). Since N_2O saturation did not decrease in scale with riverine nitrogen input, this suggests that the yield of N_2O production increased along the estuary. Dähnke et al. (2008) showed a shift from dominating denitrification towards significant nitrification in the Elbe Estuary due to the significant improvement of water quality after the reunification of Germany in 1990, and this could influence N_2O distributions in the estuary. In the following sections, we investigate the biogeochemical controls of this in-situ N_2O production. For this purpose, we discuss the two zones of intense N_2O production separately and also distinguish between cruises in spring and summer (water temperature > 10 °C) and in winter (water temperature < 6 °C).

4.2 N_2O production in spring and summer in the mesohaline estuary

The N_2O peak in the transition between oligohaline and mesohaline estuary was accompanied by a sudden change in the slope of the AOU vs N_2O_{xs} plots, (Fig. 3), pointing towards N_2O production in the oxic water column. Peaks of nitrite and ammonium concentrations coincided with the elevated nitrous oxide saturations between Elbe km 680-700, with an ammonium peak around stream kilometer ~720, and a nitrite peak at ~700 (Fig. 4a). Highest N_2O concentrations were usually measured between the nitrite peak and the region with highest turbidity (Fig. 4a, September 2020, and Fig. S4-S14). This co-occurrence of nitrite accumulation and increased N_2O saturation has been interpreted as signs for N_2O production via denitrification (e.g. Wertz et al., 2018; Sharma et al., 2022). However, denitrification does not seem likely in this oxic water column. Such a succession of nitrite and ammonium peaks is also typical for remineralization and nitrification, and the slight decrease of oxygen concentrations around the higher N_2O saturation (Fig. 2g and i) suggests oxygen consumption, possibly caused by these two processes. Sanders et al. (2018) measured small but detectable nitrification rates (1 – 2 µmol L^{-1} d^{-1}) for this region of the Elbe Estuary, suggesting that N_2O may be a side product of nitrification.
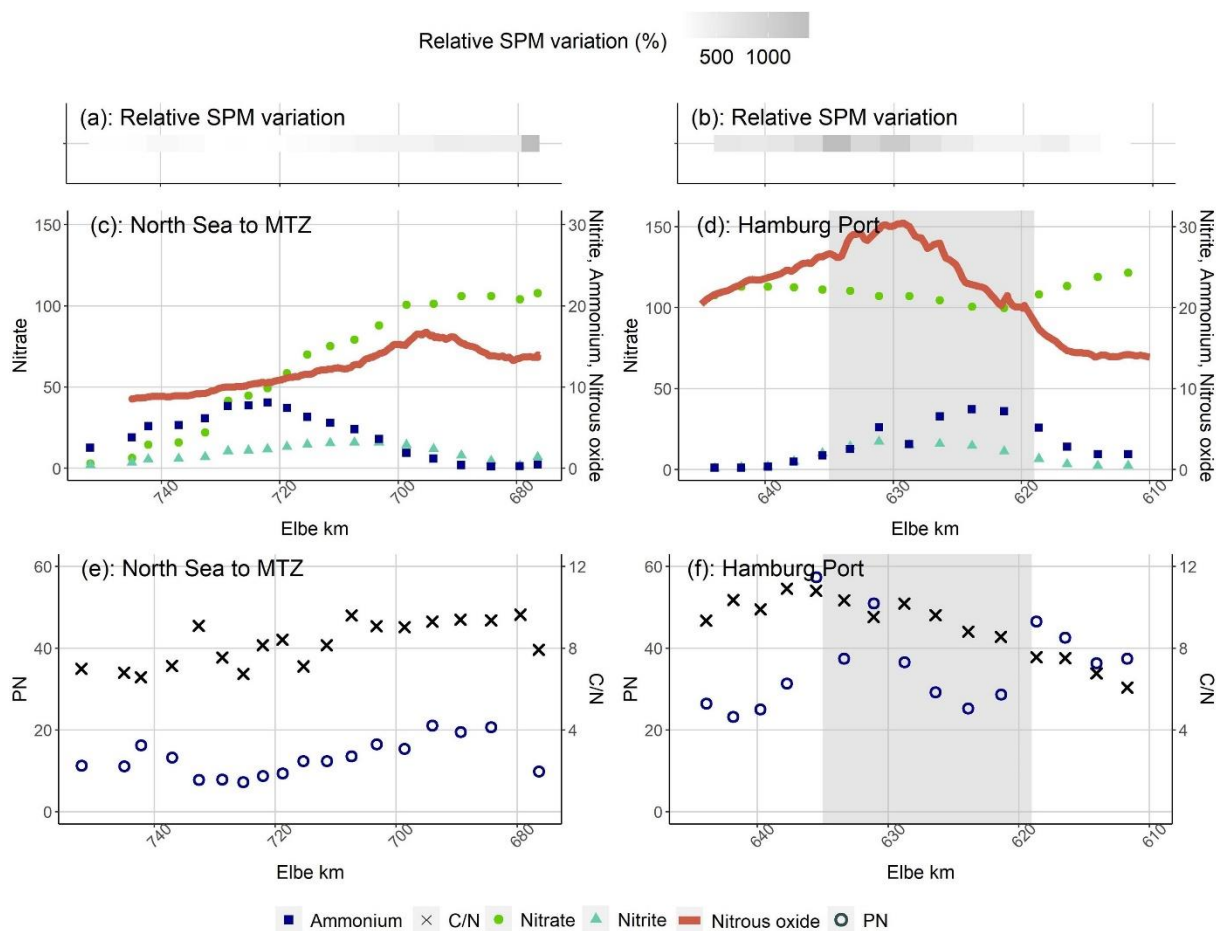
Figure 4: Succession of N-bearing substances coming from the North Sea and in the Port of Hamburg in September 2020: Relative change of SPM concentrations (a) from the North Sea and (b) in the Port of Hamburg. Nitrate in µmol L^{-1}, nitrite in µmol L^{-1}, ammonium in µmol L^{-1} and nitrous oxide concentrations in nmol L^{-1} plotted against Elbe stream kilometers (c) from the North Sea and (d) in the Port of Hamburg. Particulate nitrogen concentrations in µmol L^{-1} and C/N values plotted against stream kilometers (e) from the North Sea and (f) in the Port of Hamburg. The grey area in (d) and (f) shows the position of the Port of Hamburg.

This succession of N-bearing substances (Fig. 4, Fig. S4-S14) suggests input of particulate matter from the North Sea and upstream particle transport towards the maximum turbidity zone of the estuary (MTZ). This transport mechanism is in line with Wolfstein and Kies (1999), who explained organic matter contents and chlorophyll a concentrations in the polyhaline part of the Elbe Estuary by input of freshly produced particulate matter of marine origin. Generally, maximum turbidity zones are generated by the balance between river-induced flushing and upstream transport of marine SPM, as a function of estuarine geomorphology, gravitational circulation and tidal flow, trapping the particles in the MTZ (Bianchi, 2007; Sommerfield and Wong, 2011; Winterwerp and Wang, 2013). Other studies detected N$_2$O production from water column nitrification in estuarine MTZs (e.g. Barnes and Owens, 1999; de Wilde and de Bie, 2000; Bange, 2006; Barnes and Upstill-Goddard, 2011; Harley et al., 2015), caused by high bacterial numbers, particulate nitrogen availability and long residence times (Murray et al., 2015). For the selected dataset, we calculated a negative correlation between average SPM concentrations and N$_2$O saturation (R = -0.81, Table 5), and found that the N$_2$O peak was located downstream of the MTZ, and upstream of increasing nitrite and ammonium concentrations (Fig. 4a). This suggests that (1) the mere concentration of SPM is not the driving factor of nitrification as a source of N$_2$O, but that organic matter quality is key to biological turnover (Dähnke et al. 2022), and (2) the material transport from the North Sea upstream towards the MTZ

327 (Kappenberg and Fanger, 2007; Schoer, 1990) is a main mechanism for N_2O generation. We find organic matter

328 with low C/N ratios, and with relatively high PN and PC contents in the outermost samples (ranging from 5.9 in

329 June 2020 to 8.8 August 2017), indicating fresh and easily degradable organic matter (Fig. S1, e.g. Redfield et al.

330 1963; Fraga et al. 1998; Middelburg and Herman 2007). Towards the MTZ, C/N values, PN and PC contents

331 decreased, indicating remineralization in the water column. This remineralization and subsequent nitrification can

332 then cause the observed succession of ammonium, nitrite and N_2O peaks (Fig. 4a), contributing to the high nitrate

333 concentrations in the MTZ, where high C/N values (9 – 11/16) indicate low organic matter quality (e.g. Hedges

334 and Keil 1995; Middelburg and Herman 2007). Overall, we conclude that remineralization of marine organic

335 matter, followed by nitrification, produced the N_2O peak in the salinity gradient of the Elbe Estuary. This

336 production was mainly fueled by fresh organic matter entering the estuary from the North Sea.

337 **4.3   Hamburg Port: N_2O production in spring and summer**

338 During all cruises, we measured highest N_2O saturation in the Port of Hamburg. These peaks can be caused by

339 input from a waste water treatment plant, by deepening and dredging operations, enhanced benthic production or

340 by in-situ production in the water column.

341 Point sources generally play a minor role in the Elbe Estuary (Hofmann et al., 2005; IKSE, 2018). We estimated

342 the wastewater discharge fraction of stream flow according to Büttner et al. (2020) for the waste water treatment

343 plant (WWTP) Köhlbrandhöft, which treats the waste water from the Hamburg metropolitan region, with less than

344 5 % even under low fresh water inflow. Thus, point sources seemed not to be the cause for the elevated N_2O

345 concentrations. However, discharge of WWTPs can potentially be important sources of N_2O (Beaulieu et al., 2010;

346 Chun et al., 2020; Brown et al., 2022), and the effect of wastewater input on N_2O concentrations and emissions

347 may change with altered river discharge, water temperature and riverine nitrogen loads in the future.

348 Dredging can be a potential source of N_2O in the water column. The estuary is continuously deepened and dredged

349 to grant access for large container ships, which stirs up bottom sediments. Ammonium concentrations in the

350 sediment pore water are high (Zander et al., 2020, 2022) and N_2O can be produced by nitrifier-denitrification in

351 the sediments (Deek et al., 2013). However, we found no correlation of high SPM concentrations and N_2O

352 saturation, indicating no major influence on N_2O dynamics from channel dredging and deepening.

353 Several studies identified the Hamburg Port region as a hotspot of biogeochemical turnover: Deek et al. (2013)

354 showed denitrification, where Sanders et al. (2018) measured intense nitrification.. Norbisrath et al. (2022)

355 determined intense total alkalinity generation, and Dähnke et al. (2022) found that nitrogen turnover was driven

356 by high particulate organic matter in this region. Brase et al. (2017) identified the Hamburg port region as a hotspot

357 of N_2O production and hypothesized that simultaneous nitrification and sediment denitrification were responsible.

358 We use our expanded dataset to further evaluate this hypothesis and to identify drivers for N_2O production in the

359 port region.

360 During all cruises in spring and summer, we measured ammonium and nitrite peaks in the Hamburg Port region

361 (Fig. 2c and 2e, exemplary for September 2020 in Fig. 4b). Several researchers did address the nitrogen turnover

362 and this accumulation of nitrite and ammonium assuming that the sudden increase of water depth in the Port leads

363 to a light limitation and decomposition of riverine organic material (Schroeder, 1997; Schöl et al., 2014). This in

364 turn raises ammonium and nitrite concentrations and fosters nitrification in the port region (Sanders et al., 2018;

365 Dähnke et al., 2022).

366 High nitrite concentrations are favorable for N_2O production by nitrifier-denitrification (Quick et al., 2019), while

367 low-oxygen conditions facilitate N_2O production from both nitrification and denitrification. We found that N_2O

368 saturation increased with decreasing discharge (R = -0.48, Table 5) during spring and summer. This further points

369 towards in-situ N_2O production, because longer residence times lead to a possible accumulation of N_2O from

370 either nitrification or denitrification (e.g. Nixon et al. 1996; Pind et al. 1997; Silvennoinen et al. 2007; Gonçalves

371 et al. 2010). Overall, our data showed the succession of ammonium, nitrite and N_2O production (Fig. 4b and

372 supplementary material S4-S14) as well as a breakup of the linear relation between AOU and N_2O_{xs} in the Port

373 region (Fig. 3). In combination with previous nitrogen process studies performed in the Elbe Estuary (Deek et al.,

374 2013; Sanders et al., 2018; Dähnke et al., 2022), this supports simultaneous sedimentary denitrification and

375 nitrification in the water column as responsible pathways for N_2O production in the Port of Hamburg (Brase et al.

376 2017).

377 In spring and summer, we found no linear relationship between N_2O_{xs} and AOU in the Hamburg Port (Fig. 3). This

378 may result from combined N_2O production by nitrification and denitrification. However, oxygen saturation and

379 N_2O saturation were inversely correlated in Hamburg Port (Table 4 and 5), suggesting that N_2O production was

380 controlled by oxygen concentrations, and thus was related to oxygen consumption in the port region. Most (75 %)

381 of this oxygen consumption is caused by respiration whereas the remaining 25 % stem from nitrification (Schöl et

382 al., 2014; Sanders et al., 2018). This respiration in turn is determined by remineralization of algal material from

383 the upstream river that is transported to and respired within the port region (Schroeder, 1997; Kerner, 2000; Schöl

384 et al., 2014), linking estuarine N_2O production to river eutrophication. Fabisik et al. (2023) showed that algae could

385 additionally contribute to N_2O production. In the Elbe, fresh organic matter from the river with low C/N values as

386 well as high PN and PC contents entered the estuary. This organic material was rapidly degraded in the Hamburg

387 Port region (Fig. S1). Dähnke et al. (2022) found that labile organic matter fueled nitrification but also

388 denitrification in the fresh water part of the Elbe Estuary, which, as shown in our study, results in high N_2O

389 production in the Hamburg Port, leading to the reported negative correlations of PC and PN content with N_2O

390 saturation.

391 Overall, oxygen conditions mainly controlled N_2O production in the Hamburg Port region in spring and summer.

392 Since respiration of organic matter dominates oxygen drawdown in the port region, we deduce that N_2O production

393 there is linked to the decomposition of phytoplankton produced in the upstream Elbe River regions.

394 **4.4   Hamburg Port: N_2O production in winter**

395 In winter, low water temperature (< 6 °C) should hamper biological production (Koch et al., 1992; Halling-

396 Sorensen and Jorgensen, 1993). Indeed, we did not detect a N_2O peak in the MTZ in winter, but we find high N_2O

397 concentrations in the port region. For March 2022, we found a linear increase of N_2O_{xs} and AOU along with

398 oxygen consumption and increasing ammonium, nitrite and PN concentrations indicating nitrification in the

399 Hamburg Port producing N_2O. Unlike in summer, N_2O concentrations showed a flat increase extending far into

400 the oligohaline section of the estuary (Fig. 2, Fig. S1).

401 However, in March 2021, we found a sharp and sudden increase in N_2O, with a peak concentration that by far

402 exceeded internal biological sources in summer (Fig. 2h). An ammonium peak in the water column coincided with

403 the N_2O maximum (Fig. 2f and Fig. S12). If microbial activity is mostly temperature-inhibited, a local source of

404 N_2O in the port seems the most likely cause.

405 We considered intensified deepening operations in the Port of Hamburg as one potential source of elevated N_2O
406 saturation. Deepening and dredging work occurred in the Hamburg Port region in 2021 (HPA, pers. Comm.,
407 Karrasch 2022), but, this also applied to 2022, when we saw no sharp N_2O peak (Fig. 2h). Furthermore, the regions
408 of deepening and dredging did not match the region of high N_2O concentrations, and turbidity at the time of
409 sampling did not change significantly compared to other cruises. Jointly, this suggests that channel dredging and
410 deepening was not the primary cause for the 2021 winter N_2O peak.

411 Another possible source of N_2O is the WWTP outflow in the Southern Elbe that joins the main estuary at stream
412 kilometer 626 (Fig. 1), matching the N_2O peak at stream kilometer 627 (Fig. 2h). As explained above (section 4.3),
413 the effect of this WWTP on N_2O saturations under normal conditions should be negligible. This peak can be the
414 result of an extraordinary event during our sampling. We indeed found that an extreme rain event occurred on
415 March 11th 2021 (HAMBURG WASSER, pers. Comm., Laurich 2022) with a statistical recurrence probability of
416 one to five years (https://sri.hamburgwasser.de/, last access: 04.04.2023). This rare event caused a temperature
417 drop in the WWTP due to high inflows of cold rainwater leading to aggravated operation conditions at the time of
418 sampling. While the operators could still meet the limits for the effluent levels of nitrate and ammonium, higher
419 than usual ammonium loads exited the treatment plant at this time. We hypothesize that these elevated ammonium
420 WWTP loads were rapidly converted to N_2O as the warmer and biologically active waste water entered the Elbe
421 Estuary in March 2021. An important factor for aggravated conditions was a temperature drop in the WWTP
422 caused by cold rain water (HAMBURG WASSER, pers. Comm., Laurich 2022), we therefore hypothesize that a
423 similar rain event in warmer months would not have the same effect.

424 Therefore, we argue that our March 2021 cruise likely represents an exception due to an extreme weather situation,
425 whereas normal winter conditions in the estuary comply with the N_2O production, like in March 2022.

426 **4.5   Seasonally varying N_2O:DIN dynamic**

427 We calculated annual N_2O emissions of the Elbe Estuary ranging from 0.08 ± 0.03 Gg-N_2O yr^{-1} to
428 0.25 ± 0.16 Gg-N_2O yr^{-1}, which varied from recent N_2O summer emission estimate of 0.18 ± 0.01 Gg-N_2O yr^{-1} by
429 Brase et al. (2017). Estuarine N_2O emissions are affected by tides, diel variations and currents (Barnes et al., 2006;
430 Baulch et al., 2012; Gonçalves et al., 2015), all of which we did not address in our study. Range of possible
431 parametrizations of gas transfer coefficients further complicates a direct comparison of fluxes between studies
432 (Hall Jr. and Ulseth, 2020; Rosentreter et al., 2021), which was reflected in the big differences of our emission
433 estimates (Table 2). Therefore, a direct comparison to other studies is difficult.

434 In a more general approach, the relationship between N_2O and DIN (N_2O:DIN) is used for global estimates of N_2O
435 emissions (Kroeze et al., 2005, 2010; Ivens et al., 2011; Hu et al., 2016). Using publicly available data (Table S4
436 and S5), we calculated the amount of the annual nitrogen load released as N_2O. Depending on the parametrization
437 used for the gas transfer coefficients, 0.14 % to 0.67 % of the annual DIN loads of the Elbe Estuary were released
438 as N_2O (0.11 % to 0.57 % for TN loads). This is significantly less than the 1 % predicted by Kroeze et al. (2005),
439 but matches results from other estuaries with high agricultural input, e.g. Wells et al. (2018) with 0.3 % to 0.7 %
440 (0.1 % for TN loads) and Robinson et al. (1998) with 0.5 % (0.3 % for TN loads) as well as the 0.11 % to 0.37 %
441 estimated by Maavara et al. (2019), who used TN loads to predict global estuarine emissions. In general, N_2O:DIN
442 ratios vary widely (e.g., Baulch et al., 2012; Maavara et al., 2019; Smith and Böhlke, 2019). Wells et al. (2018)
443 even found a range from -25 % to 7 % of DIN was emitted as N_2O in estuaries with low land-use intensity. At our
444 site, highest emissions were estimated in winter (Fig. 5b) along with highest DIN loads (Fig. 5c). In spring, summer

445 and late summer, N$_2$O emissions reduced along with DIN loads (Fig. 5b, c). However, N$_2$O release did not scale

446 with the seasonal change of DIN. In winter, 0.10 % to 0.32 % of DIN were released as N$_2$O, whereas during the

447 other seasons, up to 1.26 % were emitted. Thus, our results corroborate that there is a varying relationship between

448 DIN and N$_2$O (Borges et al., 2015; Marzadri et al., 2017; Wells et al., 2018) showing that this relationship even

449 varies seasonally on site due to changing drivers for N$_2$O production and emissions, e.g., temperature (Murray et

450 al., 2015; Quick et al., 2019) and oxygen levels (de Bie et al., 2002; Rosamond et al., 2012; Yevenes et al., 2017).

451 Next to DIN loads, we find that organic matter is an important driver for N$_2$O production by providing substrate

452 for nitrification. Furthermore, the comparison of results with previous measurements in the Elbe Estuary revealed

453 that N$_2$O saturation stopped to scale with DIN input after the 1990s (section 4.1). The significant regime change

454 after the 1990s enabled phytoplankton growth to reestablish in the river that had previously been inhibited by high

455 pollutant levels and low light availability (Kerner, 2000; Amann et al., 2012; Hillebrand et al., 2018; Rewrie et al.,

456 2023). The prevailing high nitrification rates in the estuary (Dähnke et al., 2008; Sanders et al., 2018) support an

457 overarching control of organic matter on N$_2$O production and emissions along the Elbe Estuary.
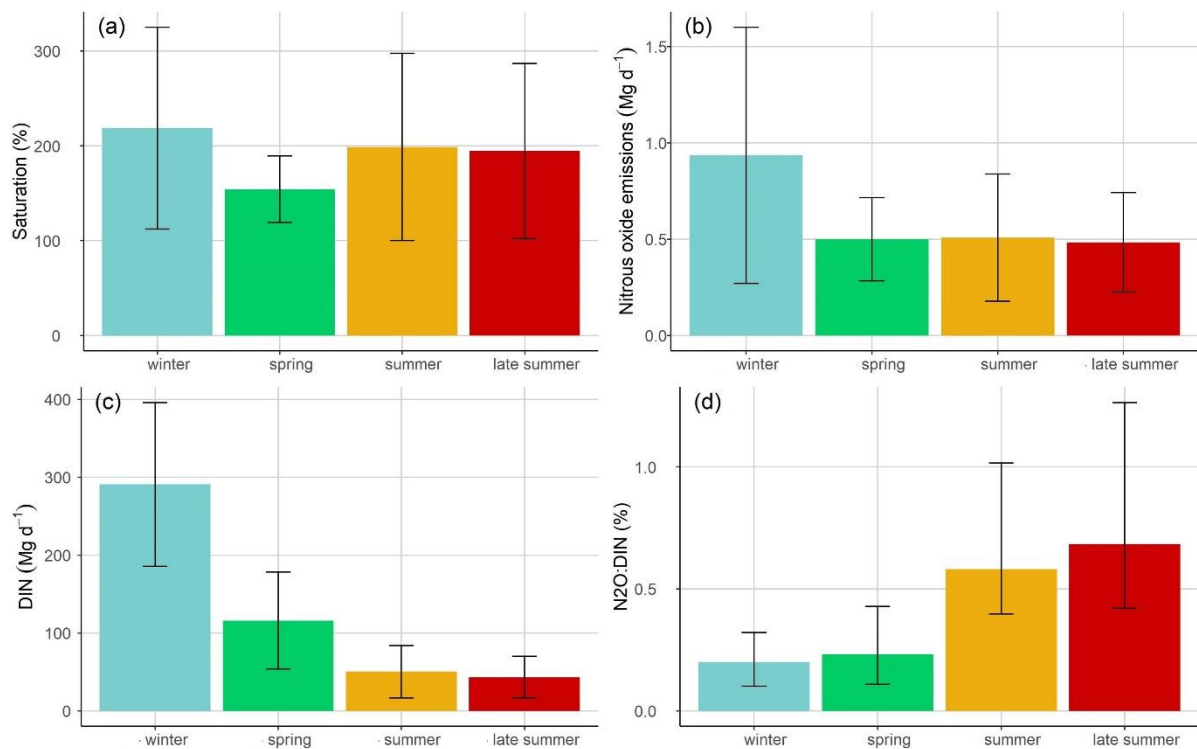
458

459 **Figure 5: (a) Average nitrous oxide saturation for each season, (b) average nitrous oxide emissions for each season**
460 **calculated after Borges et al. (2004), (c) average DIN loads for each season and (d) ratio of nitrous oxide emissions and**
461 **DIN loads (N$_2$O:DIN) for each season. The error bars represent the standard deviations for (a), (b) and (c). The**
462 **N$_2$O:DIN ratios is shown as average values calculated for each parametrization and wind speeds with error bars**
463 **representing their variability.**

464 **5   Conclusions**

465 Overall, the Elbe is a year-round source of N$_2$O to the atmosphere, with highest emissions occurring in winter,

466 along with high DIN loads and high wind speeds. However, summer N$_2$O saturation and emissions did not decrease

467 with lower riverine nitrogen input, suggesting variable relations of DIN and N$_2$O (Borges et al., 2004; Marzadri et

468 al., 2017; Wells et al., 2018), and seasonal variability of this ratio caused by changing drivers for N$_2$O production

469 and emissions. Two hot-spots of N$_2$O production were found in the Elbe Estuary: the Port of Hamburg and the

470 mesohaline estuary near the estuarine turbidity maximum. Biological N$_2$O production was fueled by riverine

organic matter in the Hamburg Port or marine organic matter in the MTZ. A comparison with historical N_2O measurements in the Elbe Estuary revealed that N_2O saturation did not decrease with DIN input after the 1990s. The improvement of water quality in the Elbe Estuary allowed phytoplankton growth after the reunification of Germany in 1990s (Kerner, 2000; Amann et al., 2012; Hillebrand et al., 2018; Rewrie et al., 2023) and led to a switch from dominant denitrification to high nitrification (Dähnke et al., 2008; Sanders et al., 2018), supporting the overarching control of organic matter on N_2O production along the Elbe Estuary. Thus, our findings indicate that DIN availability is not the sole control of N_2O production in estuaries with high agricultural input. High organic matter availability due to phytoplankton blooms driven by river eutrophication fuels nitrification and subsequent N_2O emissions, causing a decoupling of the N_2O:DIN ratio. Therefore, N_2O emissions in heavily managed estuaries with high agricultural loads are clearly linked to eutrophication. A reduced nitrogen input would reduce phytoplankton growth and thus also N_2O emissions. However, the development of phytoplankton blooms is not solely controlled by nutrient inputs, but also by e.g., temperature, residence time, water depth and grazing. Thus, complex biological and chemical processes control phytoplankton dynamics (Scharfe et al., 2009; Dijkstra et al., 2019; Kamjunke et al., 2021), which will change significantly in the future due to the effects of climate change (IPCC, 2022). A holistic approach to water quality mitigation and climate change adaptation is needed to prevent high N_2O emissions.

Data availability

The dataset generated and/or analyzed in this study are currently available upon request from the corresponding author and will be made publicly available under coastMap Geoportal (www.coastmap.org) connecting to PANGAEA. (https://www.pangaea.de/) with DOI availability in the near future.

Authors contribution

GS, TS and KD designed this study. GS did the sampling and measurements for cruises from 2020 to 2022 as well as the data interpretation and evaluation. TS was responsible for the sampling and measurements for cruises done in 2017 and 2019. YGV provided the oxygen data correction from the FerryBox data. KD, HWB, YGV and TS contributed with scientific and editorial recommendations. GS prepared the manuscript with contributions of all co-authors.

Competing interest

The authors declare that they have no conflict of interest.

Acknowledgments

References

Amann, T., Weiss, A., and Hartmann, J.: Carbon dynamics in the freshwater part of the Elbe estuary, Germany: Implications of improving water quality, Estuar. Coast. Shelf Sci., 107, 112–121, https://doi.org/10.1016/j.ecss.2012.05.012, 2012.

Bange, H. W.: Nitrous oxide and methane in European coastal waters, Estuar. Coast. Shelf Sci., 70, 361–374, https://doi.org/10.1016/j.ecss.2006.05.042, 2006.

Bange, H. W.: Chapter 2 - Gaseous Nitrogen Compounds (NO, N_2O, N_2, NH_3) in the Ocean, Nitrogen Mar. Environ. Second Ed., 51–94, https://doi.org/10.1016/B978-0-12-372522-6.00002-5, 2008.

Barnes, J. and Owens, N. J. P.: Denitrification and Nitrous Oxide Concentrations in the Humber Estuary, UK, and Adjacent Coastal Zones, Mar. Pollut. Bull., 37, 247–260, https://doi.org/10.1016/S0025-326X(99)00079-X, 1999.

Barnes, J. and Upstill-Goddard, R. C.: N_2O seasonal distributions and air-sea exchange in UK estuaries: Implications for the tropospheric N_2O source from European coastal waters, J. Geophys. Res. Biogeosciences, 116, https://doi.org/10.1029/2009JG001156, 2011.

Barnes, J., Ramesh, R., Purvaja, R., Nirmal Rajkumar, A., Senthil Kumar, B., Krithika, K., Ravichandran, K., Uher, G., and Upstill-Goddard, R.: Tidal dynamics and rainfall control N_2O and CH_4 emissions from a pristine mangrove creek, Geophys. Res. Lett., 33, https://doi.org/10.1029/2006GL026829, 2006.

Baulch, H. M., Dillon, P. J., Maranger, R., Venkiteswaran, J. J., Wilson, H. F., and Schiff, S. L.: Night and day: short-term variation in nitrogen chemistry and nitrous oxide emissions from streams, Freshw. Biol., 57, 509–525, https://doi.org/10.1111/j.1365-2427.2011.02720.x, 2012.

BAW Oritz, V.: pers. Comm.: Flächen des Elbe Ästuars, 2023.

Beaulieu, J. J., Shuster, W. D., and Rebholz, J. A.: Nitrous Oxide Emissions from a Large, Impounded River: The Ohio River, Environ. Sci. Technol., 44, 7527–7533, https://doi.org/10.1021/es1016735, 2010.

Bergemann, M.: Die Trübungszone in der Tideelbe - Beschreibung der räumlichen und zeitlichen Entwicklung, Wassergütestelle Elbe, 2004.

Bergemann, M. and Gaumert, T.: Elbebericht 2008: Ergebnisse des nationalen Überwachungsprogramms Elbe der Bundesländerüber den ökologischen und chemischen Zustand der Elbe nach EG-WRRLsowie der Trendentwicklung von Stoffen und Schadstoffgruppen, Flussgebietsgemeinschaft Elbe (FGG Elbe), Hamburg, 2008.

van Beusekom, J. E. E., Carstensen, J., Dolch, T., Grage, A., Hofmeister, R., Lenhart, H., Kerimoglu, O., Kolbe, K., Pätsch, J., Rick, J., Rönn, L., and Ruiter, H.: Wadden Sea Eutrophication: Long-Term Trends and Regional Differences, Front. Mar. Sci., 6, 370, https://doi.org/10.3389/fmars.2019.00370, 2019.

Bianchi, T. S.: Biogeochemistry of Estuaries, Oxford University Press, New York, 706 pp., https://doi.org/10.1093/oso/9780195160826.001.0001, 2007.

de Bie, M. J. M., Middelburg, J. J., Starink, M., and Laanbroek, H. J.: Factors controlling nitrous oxide at the microbial community and estuarine scale, Mar. Ecol. Prog. Ser., 240, 1–9, https://doi.org/10.3354/meps240001, 2002.

Boehlich, M. J. and Strotmann, T.: The Elbe Estuary, Küste, 74, 288–306, 2008.

Boehlich, M. J. and Strotmann, T.: Das Elbeästuar, Küste, 87, Kuratorium für Forschung im Küsteningenieurwesen (KFKI), https://doi.org/10.18171/1.087106, 2019.

Borges, A., Vanderborght, J.-P., Schiettecatte, L.-S., Gazeau, F., Ferrón-Smith, S., Delille, B., and Frankignoulle, M.: Variability of gas transfer velocity of CO_2 in a macrotidal estuary (The Scheldt), Estuaries, 27, 593–603, https://doi.org/10.1007/BF02907647, 2004.

Borges, A. V., Darchambeau, F., Teodoru, C. R., Marwick, T. R., Tamooh, F., Geeraert, N., Omengo, F. O., Guérin, F., Lambert, T., Morana, C., Okuku, E., and Bouillon, S.: Globally significant greenhouse-gas emissions from African inland waters, Nat. Geosci., 8, 637–642, https://doi.org/10.1038/ngeo2486, 2015.

Bouwman, A. F., Bierkens, M. F. P., Griffioen, J., Hefting, M. M., Middelburg, J. J., Middelkoop, H., and Slomp, C. P.: Nutrient dynamics, transfer and retention along the aquatic continuum from land to ocean: towards integration of ecological and biogeochemical models, Biogeosciences, 10, 1–23, https://doi.org/10.5194/bg-10-1-2013, 2013.

Brase, L., Bange, H. W., Lendt, R., Sanders, T., and Dähnke, K.: High Resolution Measurements of Nitrous Oxide (N_2O) in the Elbe Estuary, Front. Mar. Sci., 4, 162, https://doi.org/10.3389/fmars.2017.00162, 2017.

Brown, A. M., Bass, A. M., and Pickard, A. E.: Anthropogenic-estuarine interactions cause disproportionate greenhouse gas production: A review of the evidence base, Mar. Pollut. Bull., 174, 113240, https://doi.org/10.1016/j.marpolbul.2021.113240, 2022.

Büttner, O., Jawitz, J. W., and Borchardt, D.: Ecological status of river networks: stream order-dependent impacts of agricultural and urban pressures across ecoregions, Environ. Res. Lett., 15, 1040b3, https://doi.org/10.1088/1748-9326/abb62e, 2020.

Chun, Y., Kim, D., Hattori, S., Toyoda, S., Yoshida, N., Huh, J., Lim, J.-H., and Park, J.-H.: Temperature control on wastewater and downstream nitrous oxide emissions in an urbanized river system, Water Res., 187, 116417, https://doi.org/10.1016/j.watres.2020.116417, 2020.

Clark, J. F., Schlosser, P., Simpson, H. J., Stute, M., Wanninkhof, R., and Ho, D. T.: Relationship between gas transfer velocities and wind speeds in the tidal Hudson River determined by the dual tracer technique, in: Air-Water Gas Transfer, edited by: Jähne, B. and Monahan, E. C., AEON Verlag, Hanau, 785–800, 1995.

Crossland, C. J., Baird, D., Ducrotoy, J.-P., Lindeboom, H., Buddemeier, R. W., Dennison, W. C., Maxwell, B. A., Smith, S. V., and Swaney, D. P.: The Coastal Zone — a Domain of Global Interactions, in: Coastal Fluxes in the Anthropocene: The Land-Ocean Interactions in the Coastal Zone Project of the International Geosphere-Biosphere Programme, edited by: Crossland, C. J., Kremer, H. H., Lindeboom, H. J., Marshall Crossland, J. I., and Tissier, M. D. A., Springer, Berlin, Heidelberg, 1–37, https://doi.org/10.1007/3-540-27851-6_1, 2005.

Dähnke, K., Bahlmann, E., and Emeis, K.-C.: A nitrate sink in estuaries? An assessment by means of stable nitrate isotopes in the Elbe estuary, Limnol. Oceanogr., 53, 1504–1511, https://doi.org/10.4319/lo.2008.53.4.1504, 2008.

Dähnke, K., Sanders, T., Voynova, Y., and Wankel, S. D.: Nitrogen isotopes reveal a particulate-matter-driven biogeochemical reactor in a temperate estuary, Biogeosciences, 19, 5879–5891, https://doi.org/10.5194/bg-19-5879-2022, 2022.

Deek, A., Dähnke, K., van Beusekom, J., Meyer, S., Voss, M., and Emeis, K.-C.: N2 fluxes in sediments of the Elbe Estuary and adjacent coastal zones, Mar. Ecol. Prog. Ser., 493, 9–21, https://doi.org/10.3354/meps10514, 2013.

Dijkstra, Y. M., Chant, R. J., and Reinfelder, J. R.: Factors Controlling Seasonal Phytoplankton Dynamics in the Delaware River Estuary: an Idealized Model Study, Estuaries Coasts, 42, 1839–1857, https://doi.org/10.1007/s12237-019-00612-3, 2019.

592 Dlugokencky, E. J., Crotwell, A. M., Mund, J. W., Crotwell, M. J., and Thoning, K. W.: Earth System Research
593 Laboratory Carbon Cycle and Greenhouse Gases Group Flask-Air Sample Measurements of N_2O at Global and
594 Regional Background Sites, 1967-Present [Data set], https://doi.org/10.15138/53G1-X417, 2022.

595 Fabisik, F., Guieysse, B., Procter, J., and Plouviez, M.: Nitrous oxide (N_2O) synthesis by the freshwater
596 cyanobacterium Microcystis aeruginosa, Biogeosciences, 20, 687–693, https://doi.org/10.5194/bg-20-687-2023,
597 2023.

598 FGG Elbe: Naehrstoffminderungsstrategie für die Flussgebietsgemeinschaft Elbe, Flussgebietsgemeinschaft Elbe
599 (FGG Elbe), Magdeburg, 2018.

600 Das Fachinfomrationssystem (FIS) der FGG Elbe: https://www.elbe-
601 datenportal.de/FisFggElbe/content/start/ZurStartseite.action;jsessionid=A37EDCF5B5EC1ECB15091447E64EC
602 538, last access: 21 November 2022.

603 Fraga, F., Ríos, A. F., Pérez, F. F., and Figueiras, F. G.: Theoretical limits of oxygen:carbon and oxygen:nitrogen
604 ratios during photosynthesis and mineralisation of organic matter in the sea, Sci. Mar., 62, 161–168,
605 https://doi.org/10.3989/scimar.1998.62n1-2161, 1998.

606 Garnier, J., Cébron, A., Tallec, G., Billen, G., Sebilo, M., and Martinez, A.: Nitrogen Behaviour and Nitrous Oxide
607 Emission in the Tidal Seine River Estuary (France) as Influenced by Human Activities in the Upstream Watershed,
608 Biogeochemistry, 77, 305–326, https://doi.org/10.1007/s10533-005-0544-4, 2006.

609 Gaumert, T. and Bergemann, M.: Sauerstoffgehalt der Tideelbe - Entwicklung der kritischen Sauerstoffgehalte im
610 Jahr 2007 und in den Vorjahren, Erörterung möglicher Ursachen und Handlungsoptionen,
611 Flussgebietsgemeinschaft Elbe, 2007.

612 Geerts, L., Wolfstein, K., Jacobs, S., van Damme, S., and Vandenbruwaene, W.: Zonation of the TIDE estuaries,
613 TIDE toolbox, 2012.

614 Gonçalves, C., Brogueira, M. J., and Camões, M. F.: Seasonal and tidal influence on the variability of nitrous oxide
615 in the Tagus estuary, Portugal, Sci. Mar., 74, 57–66, https://doi.org/10.3989/scimar.2010.74s1057, 2010.

616 Gonçalves, C., Brogueira, M. J., and Nogueira, M.: Tidal and spatial variability of nitrous oxide (N_2O) in Sado
617 estuary (Portugal), Estuar. Coast. Shelf Sci., 167, 466–474, https://doi.org/10.1016/j.ecss.2015.10.028, 2015.

618 Hall Jr., R. O. and Ulseth, A. J.: Gas exchange in streams and rivers, WIREs Water, 7, e1391,
619 https://doi.org/10.1002/wat2.1391, 2020.

620 Halling-Sorensen, B. and Jorgensen, S. E. (Eds.): 3. Process Chemistry and Biochemistry of Nitrification, in:
621 Studies in Environmental Science, vol. 54, Elsevier, 55–118, https://doi.org/10.1016/S0166-1116(08)70525-9,
622 1993.

623 HAMBURG WASSER, Laurich, F.: pers. Comm.: N_2O in der Elbe, 2022.

624 Hanke, V.-R. and Knauth, H.-D.: N_2O-Gehalte in Wasser-und Luftproben aus den Bereichen der Tideelbe und der
625 Deutschen Bucht, GKSS-Forschungszentrum, Weinheim, 1990.

626 Hansen, H. P. and Koroleff, F.: Determination of nutrients, in: Methods of Seawater Analysis, John Wiley & Sons,
627 Ltd, 159–228, https://doi.org/10.1002/9783527613984.ch10, 1999.

628 Harley, J. F., Carvalho, L., Dudley, B., Heal, K. V., Rees, R. M., and Skiba, U.: Spatial and seasonal fluxes of the
629 greenhouse gases N_2O, CO_2 and CH_4 in a UK macrotidal estuary, Estuar. Coast. Shelf Sci., 153, 62–73,
630 https://doi.org/10.1016/j.ecss.2014.12.004, 2015.

631 Hedges, J. I. and Keil, R. G.: Sedimentary organic matter preservation: an assessment and speculative synthesis,
632 Mar. Chem., 49, 81–115, https://doi.org/10.1016/0304-4203(95)00008-F, 1995.

633 Hein, S. S. V., Sohrt, V., Nehlsen, E., Strotmann, T., and Fröhle, P.: Tidal Oscillation and Resonance in Semi-
634 Closed Estuaries—Empirical Analyses from the Elbe Estuary, North Sea, Water, 13, 848,
635 https://doi.org/10.3390/w13060848, 2021.

636 Schleswig-Holstein u. Hamburg: Mittlere Windgeschwindigkeit (1986-2015)* | Norddeutscher Klimamonitor:
637 https://www.norddeutscher-klimamonitor.de/klima/1986-2015/jahr/mittlere-windgeschwindigkeit/schleswig-
638 holstein-hamburg/coastdat-1.html, last access: 27 April 2023.

639 Hillebrand, G., Hardenbicker, P., Fischer, H., Otto, W., and Vollmer, S.: Dynamics of total suspended matter and
640 phytoplankton loads in the river Elbe, J. Soils Sediments, 18, 3104–3113, https://doi.org/10.1007/s11368-018-
641 1943-1, 2018.

642 Hofmann, J., Behrendt, H., Gilbert, A., Janssen, R., Kannen, A., Kappenberg, J., Lenhart, H., Lise, W., Nunneri,
643 C., and Windhorst, W.: Catchment–coastal zone interaction based upon scenario and model analysis: Elbe and the
644 German Bight case study, Reg. Environ. Change, 5, 54–81, https://doi.org/10.1007/s10113-004-0082-y, 2005.

645 HPA and Freie und Hansestadt Hamburg: Deutsches Gewässerkundliches Jahrbuch - Elbegebiet, Teil III, Untere
646 Elbe ab der Havelmündung - 2014, Hamburg, 2017.

647 HPA, Karrasch, M.: pers. Comm.: Anfrage wegen N_2O Peak - Baggerarbeiten Elbe März 2021 und März 2022,
648 2022.

649 Hu, M., Chen, D., and Dahlgren, R. A.: Modeling nitrous oxide emission from rivers: a global assessment, Glob.
650 Change Biol., 22, 3566–3582, https://doi.org/10.1111/gcb.13351, 2016.

651 IKSE: Strategie zur Minderung der Nährstoffeinträge in Gewässer in der internationalen Flussgebietsgemeinschaft
652 Elbe, Internationale Kommission zur Schutz der Elbe, Magdeburg, 2018.

653 IPCC: Climate Change 2021: The Physical Science Basis. Contribution of Working Group I to the Sixth
654 Assessment Report of the Intergovernmental Panel on Climate Change, edited by: Masson-Delmotte, V., Zhai, P.,
655 Pirani, A., Connors, S. L., Péan, C., Berger, S., Caud, N., Chen, Y., Goldfarb, L., Gomis, M. I., Huang, M., Leitzell,
656 K., Lonnoy, E., Matthews, J. B. R., Maycock, T. K., Waterfield, T., Yelekçi, Ö., Yu, R., and Zhou, B., Cambridge
657 University Press, Cambridge, United Kingdom and New York, NY, USA,
658 https://doi.org/10.1017/9781009157896, 2021.

659 IPCC: Climate Change 2022: Impacts, Adaptation and Vulnerability. Contribution of Working Group II to the
660 Sixth Assessment Report of the Intergovernmental Panel on Climate Change., edited by: Pörtner, H.-O., Roberts,
661 D. C., Tignor, M. M. B., Poloczanska, E. S., Mintenbeck, K., Alegría, A., Craig, M., Langsdorf, S., Löschke, S.,
662 Möller, V., Okem, A., and Rama, B., Cambridge University Press, Cambridge, UK and New York, NY, USA,
663 3056 pp., https://doi.org/10.1017/9781009325844, 2022.

664 Ivens, W. P. M. F., Tysmans, D. J. J., Kroeze, C., Löhr, A. J., and van Wijnen, J.: Modeling global N_2O emissions
665 from aquatic systems, Curr. Opin. Environ. Sustain., 3, 350–358, https://doi.org/10.1016/j.cosust.2011.07.007,
666 2011.

667 Ji, Q., Frey, C., Sun, X., Jackson, M., Lee, Y.-S., Jayakumar, A., Cornwell, J. C., and Ward, B. B.: Nitrogen and
668 oxygen availabilities control water column nitrous oxide production during seasonal anoxia in the Chesapeake
669 Bay, Biogeosciences, 15, 6127–6138, https://doi.org/10.5194/bg-15-6127-2018, 2018.

670 Johannsen, A., Dähnke, K., and Emeis, K.: Isotopic composition of nitrate in five German rivers discharging into
671 the North Sea, Org. Geochem., 39, 1678–1689, https://doi.org/10.1016/j.orggeochem.2008.03.004, 2008.

672 Kamjunke, N., Rode, M., Baborowski, M., Kunz, J., Zehner, J., Borchardt, D., and Weitere, M.: High irradiation
673 and low discharge promote the dominant role of phytoplankton in riverine nutrient dynamics, Limnol. Oceanogr.,
674 66, https://doi.org/10.1002/lno.11778, 2021.

675 Kappenberg, J. and Fanger, H.-U.: Sedimenttransportgeschehen in der tidebeeinflussten Elbe, der Deutschen Bucht
676 und in der Nordsee, GKSS-Forschungszentrum, Geesthacht, 2007.

677 Kassambara, A.: ggpubr: "ggplot2" Based Publication Ready Plots, 2023.

678 Kerner, M.: Interactions between local oxygen deficiencies and heterotrophic microbial processes in the elbe
679 estuary, Limnologica, 30, 137–143, https://doi.org/10.1016/S0075-9511(00)80008-0, 2000.

680 Knowles, R.: Denitrification, Microbiol. Rev., 46, 43–70, https://doi.org/10.1128/mr.46.1.43-70.1982, 1982.

681 Koch, M. S., Maltby, E., Oliver, G. A., and Bakker, S. A.: Factors controlling denitrification rates of tidal mudflats
682 and fringing salt marshes in south-west England, Estuar. Coast. Shelf Sci., 34, 471–485,
683 https://doi.org/10.1016/S0272-7714(05)80118-0, 1992.

684 Kroeze, C., Dumont, E., and Seitzinger, S. P.: New estimates of global emissions of N_2O from rivers and estuaries,
685 Environ. Sci., 2, 159–165, https://doi.org/10.1080/15693430500384671, 2005.

686 Kroeze, C., Dumont, E., and Seitzinger, S.: Future trends in emissions of N_2O from rivers and estuaries, J. Integr.
687 Environ. Sci., 7, 71–78, https://doi.org/10.1080/1943815X.2010.496789, 2010.

688 Maavara, T., Lauerwald, R., Laruelle, G. G., Akbarzadeh, Z., Bouskill, N. J., Van Cappellen, P., and Regnier, P.:
689 Nitrous oxide emissions from inland waters: Are IPCC estimates too high?, Glob. Change Biol., 25, 473–488,
690 https://doi.org/10.1111/gcb.14504, 2019.

691 Marzadri, A., Dee, M. M., Tonina, D., Bellin, A., and Tank, J. L.: Role of surface and subsurface processes in
692 scaling N_2O emissions along riverine networks, Proc. Natl. Acad. Sci., 114, 4330–4335,
693 https://doi.org/10.1073/pnas.1617454114, 2017.

694 Middelburg, J. J. and Herman, P. M. J.: Organic matter processing in tidal estuaries, Mar. Chem., 106, 127–147,
695 https://doi.org/10.1016/j.marchem.2006.02.007, 2007.

696 Middelburg, J. J. and Nieuwenhuize, J.: Uptake of dissolved inorganic nitrogen in turbid, tidal estuaries, Mar.
697 Ecol.-Prog. Ser., 192, 79–88, https://doi.org/10.3354/meps192079, 2000.

698 Murray, R. H., Erler, D. V., and Eyre, B. D.: Nitrous oxide fluxes in estuarine environments: response to global
699 change, Glob. Change Biol., 21, 3219–3245, https://doi.org/10.1111/gcb.12923, 2015.

700 Nevison, C., Butler, J. H., and Elkins, J. W.: Global distribution of N_2O and the ΔN_2O-AOU yield in the subsurface
701 ocean, Glob. Biogeochem. Cycles, 17, 1119, https://doi.org/10.1029/2003GB002068, 2003.

702 Nightingale, P. D., Malin, G., Law, C. S., Watson, A. J., Liss, P. S., Liddicoat, M. I., Boutin, J., and Upstill-
703 Goddard, R. C.: In situ evaluation of air-sea gas exchange parameterizations using novel conservative and volatile
704 tracers, Glob. Biogeochem. Cycles, 14, 373–387, https://doi.org/10.1029/1999GB900091, 2000.

705 Nixon, S. W., Ammerman, J. W., Atkinson, L. P., Berounsky, V. M., Billen, G., Boicourt, W. C., Boynton, W. R.,
706 Church, T. M., Ditoro, D. M., Elmgren, R., Garber, J. H., Giblin, A. E., Jahnke, R. A., Owens, N. J. P., Pilson, M.
707 E. Q., and Seitzinger, S. P.: The fate of nitrogen and phosphorus at the land-sea margin of the North Atlantic
708 Ocean, Biogeochemistry, 35, 141–180, https://doi.org/10.1007/BF02179826, 1996.

709 Norbisrath, M., Pätsch, J., Dähnke, K., Sanders, T., Schulz, G., van Beusekom, J. E. E., and Thomas, H.: Metabolic
710 alkalinity release from large port facilities (Hamburg, Germany) and impact on coastal carbon storage,
711 Biogeosciences, 19, 5151–5165, https://doi.org/10.5194/bg-19-5151-2022, 2022.

712 Pätsch, J., Serna, A., Dähnke, K., Schlarbaum, T., Johannsen, A., and Emeis, K.-C.: Nitrogen cycling in the
713 German Bight (SE North Sea) — Clues from modelling stable nitrogen isotopes, Cont. Shelf Res., 30, 203–213,
714 https://doi.org/10.1016/j.csr.2009.11.003, 2010.

715 Pind, A., Risgaard-Petersen, N., and Revsbech, N. P.: Denitrification and microphytobenthic NO_3^- consumption
716 in a Danish lowland stream: diurnal and seasonal variation, Aquat. Microb. Ecol., 12, 275–284,
717 https://doi.org/10.3354/ame012275, 1997.

718 Quick, A. M., Reeder, W. J., Farrell, T. B., Tonina, D., Feris, K. P., and Benner, S. G.: Nitrous oxide from streams
719 and rivers: A review of primary biogeochemical pathways and environmental variables, Earth-Sci. Rev., 191, 224–
720 262, https://doi.org/10.1016/j.earscirev.2019.02.021, 2019.

721 Quiel, K., Becker, A., Kirchesch, V., Schöl, A., and Fischer, H.: Influence of global change on phytoplankton and
722 nutrient cycling in the Elbe River, Reg. Environ. Change, 11, 405–421, https://doi.org/10.1007/s10113-010-0152-
723 2, 2011.

724 The R Stats Package, Version 4.0.2:
725 https://www.rdocumentation.org/packages/stats/versions/3.6.2/topics/prcomp, last access: 29 January 2021.

Radach, G. and Pätsch, J.: Variability of continental riverine freshwater and nutrient inputs into the North Sea for the years 1977–2000 and its consequences for the assessment of eutrophication, Estuaries Coasts, 30, 66–81, https://doi.org/10.1007/BF02782968, 2007.

Reading, M. J., Tait, D. R., Maher, D. T., Jeffrey, L. C., Looman, A., Holloway, C., Shishaye, H. A., Barron, S., and Santos, I. R.: Land use drives nitrous oxide dynamics in estuaries on regional and global scales, Limnol. Oceanogr., 65, 1903–1920, https://doi.org/10.1002/lno.11426, 2020.

Redfield, A. C., Ketchum, B. H., and Richards, F. A.: The influence of organisms on the composition of sea-water, Compos. Seawater Comp. Descr. Oceanogr. Sea Ideas Obs. Prog. Study Seas, 2, 26–77, 1963.

Rewrie, L. C. V., Voynova, Y. G., van Beusekom, J. E. E., Sanders, T., Körtzinger, A., Brix, H., Ollesch, G., and Baschek, B.: Significant shifts in inorganic carbon and ecosystem state in a temperate estuary (1985–2018), Limnol. Oceanogr., in press, https://doi.org/10.1002/lno.12395, 2023.

Rhee, T. S.: The process of air -water gas exchange and its application, Texas A&M University, College Station, 2000.

Rhee, T. S., Kettle, A. J., and Andreae, M. O.: Methane and nitrous oxide emissions from the ocean: A reassessment using basin-wide observations in the Atlantic, J. Geophys. Res. Atmospheres, 114, D12304, https://doi.org/10.1029/2008JD011662, 2009.

Robinson, A. D., Nedwell, D. B., Harrison, R. M., and Ogilvie, B. G.: Hypernutrified estuaries as sources of N$_2$O emission to the atmosphere: the estuary of the River Colne, Essex, UK, Mar. Ecol. Prog. Ser., 164, 59–71, https://doi.org/10.3354/meps164059, 1998.

Rosamond, M. S., Thuss, S. J., and Schiff, S. L.: Dependence of riverine nitrous oxide emissions on dissolved oxygen levels, Nat. Geosci., 5, 715–718, https://doi.org/10.1038/ngeo1556, 2012.

Rosenhagen, G., Schatzmann, M., and Schrön, A.: Das Klima der Metropolregion auf Grundlage meteorologischer Messungen und Beobachtungen, in: Klimabericht für die Metropolregion Hamburg, edited by: von Storch, H. and Claussen, M., Springer, Berlin, Heidelberg, 19–59, https://doi.org/10.1007/978-3-642-16035-6_2, 2011.

Rosentreter, J. A., Wells, N. S., Ulseth, A. J., and Eyre, B. D.: Divergent Gas Transfer Velocities of CO_2, CH_4, and N_2O Over Spatial and Temporal Gradients in a Subtropical Estuary, J. Geophys. Res. Biogeosciences, 126, e2021JG006270, https://doi.org/10.1029/2021JG006270, 2021.

Sanders, T., Schöl, A., and Dähnke, K.: Hot Spots of Nitrification in the Elbe Estuary and Their Impact on Nitrate Regeneration, Estuaries Coasts, 41, 128–138, https://doi.org/10.1007/s12237-017-0264-8, 2018.

Scharfe, M., Callies, U., Blöcker, G., Petersen, W., and Schroeder, F.: A simple Lagrangian model to simulate temporal variability of algae in the Elbe River, Ecol. Model., 220, 2173–2186, https://doi.org/10.1016/j.ecolmodel.2009.04.048, 2009.

Schoer, J. H.: Determination of the origin of suspended matter and sediments in the Elbe estuary using natural tracers, Estuaries, 13, 161–172, https://doi.org/10.2307/1351585, 1990.

Schöl, A., Hein, B., Wyrwa, J., and Kirchesch, V.: Modelling Water Quality in the Elbe and its Estuary – Large Scale and Long Term Applications with Focus on the Oxygen Budget of the Estuary, Küste, 203–232, 2014.

Schroeder, F.: Water quality in the Elbe estuary: Significance of different processes for the oxygen deficit at Hamburg, Environ. Model. Assess., 2, 73–82, https://doi.org/10.1023/A:1019032504922, 1997.

Sharma, N., Flynn, E. D., Catalano, J. G., and Giammar, D. E.: Copper availability governs nitrous oxide accumulation in wetland soils and stream sediments, Geochim. Cosmochim. Acta, 327, 96–115, https://doi.org/10.1016/j.gca.2022.04.019, 2022.

Siedler, G. and Peters, H.: Properties of sea water, Physical properties, in: Oceanography, vol. V/3a, edited by: Sündermann, J., Springer, Berlin, Germany, 233–264, 1986.

769 Silvennoinen, H., Hietanen, S., Liikanen, A., Stange, C. F., Russow, R., Kuparinen, J., and Martikainen, P. J.:
770 Denitrification in the River Estuaries of the Northern Baltic Sea, AMBIO J. Hum. Environ., 36, 134–140,
771 https://doi.org/10.1579/0044-7447(2007)36[134:DITREO]2.0.CO;2, 2007.

772 Smith, R. L. and Böhlke, J. K.: Methane and nitrous oxide temporal and spatial variability in two midwestern USA
773 streams containing high nitrate concentrations, Sci. Total Environ., 685, 574–588,
774 https://doi.org/10.1016/j.scitotenv.2019.05.374, 2019.

775 Sommerfield, C. K. and Wong, K.-C.: Mechanisms of sediment flux and turbidity maintenance in the Delaware
776 Estuary, J. Geophys. Res. Oceans, 116, C01005, https://doi.org/10.1029/2010JC006462, 2011.

777 Tang, W., Tracey, J. C., Carroll, J., Wallace, E., Lee, J. A., Nathan, L., Sun, X., Jayakumar, A., and Ward, B. B.:
778 Nitrous oxide production in the Chesapeake Bay, Limnol. Oceanogr., 67, 2101–2116,
779 https://doi.org/10.1002/lno.12191, 2022.

780 Tian, H., Xu, R., Canadell, J. G., Thompson, R. L., Winiwarter, W., Suntharalingam, P., Davidson, E. A., Ciais,
781 P., Jackson, R. B., Janssens-Maenhout, G., Prather, M. J., Regnier, P., Pan, N., Pan, S., Peters, G. P., Shi, H.,
782 Tubiello, F. N., Zaehle, S., Zhou, F., Arneth, A., Battaglia, G., Berthet, S., Bopp, L., Bouwman, A. F., Buitenhuis,
783 E. T., Chang, J., Chipperfield, M. P., Dangal, S. R. S., Dlugokencky, E., Elkins, J. W., Eyre, B. D., Fu, B., Hall,
784 B., Ito, A., Joos, F., Krummel, P. B., Landolfi, A., Laruelle, G. G., Lauerwald, R., Li, W., Lienert, S., Maavara,
785 T., MacLeod, M., Millet, D. B., Olin, S., Patra, P. K., Prinn, R. G., Raymond, P. A., Ruiz, D. J., van der Werf, G.
786 R., Vuichard, N., Wang, J., Weiss, R. F., Wells, K. C., Wilson, C., Yang, J., and Yao, Y.: A comprehensive
787 quantification of global nitrous oxide sources and sinks, Nature, 586, 248–256, https://doi.org/10.1038/s41586-
788 020-2780-0, 2020.

789 US EPA: Volunteer Estuary Monitoring: A Methods Manual, United States Environmental Protection Agency
790 (EPA), 2006.

791 Walter, S., Bange, H. W., and Wallace, D. W. R.: Nitrous oxide in the surface layer of the tropical North Atlantic
792 Ocean along a west to east transect, Geophys. Res. Lett., 31, L23S07, https://doi.org/10.1029/2004GL019937,
793 2004.

794 Wanninkhof, R.: Relationship between wind speed and gas exchange over the ocean, J. Geophys. Res. Oceans, 97,
795 7373–7382, https://doi.org/10.1029/92JC00188, 1992.

796 Weiss, R. F.: The solubility of nitrogen, oxygen and argon in water and seawater, Deep Sea Res. Oceanogr. Abstr.,
797 17, 721–735, https://doi.org/10.1016/0011-7471(70)90037-9, 1970.

798 Weiss, R. F. and Price, B. A.: Nitrous oxide solubility in water and seawater, Mar. Chem., 8, 347–359,
799 https://doi.org/10.1016/0304-4203(80)90024-9, 1980.

800 Wells, N. S., Maher, D. T., Erler, D. V., Hipsey, M., Rosentreter, J. A., and Eyre, B. D.: Estuaries as Sources and
801 Sinks of N_2O Across a Land Use Gradient in Subtropical Australia, Glob. Biogeochem. Cycles, 32, 877–894,
802 https://doi.org/10.1029/2017GB005826, 2018.

803 Wertz, S., Goyer, C., Burton, D. L., Zebarth, B. J., and Chantigny, M. H.: Processes contributing to nitrite
804 accumulation and concomitant N_2O emissions in frozen soils, Soil Biol. Biochem., 126, 31–39,
805 https://doi.org/10.1016/j.soilbio.2018.08.001, 2018.

806 de Wilde, H. P. and de Bie, M. J.: Nitrous oxide in the Schelde estuary: production by nitrification and emission
807 to the atmosphere, Mar. Chem., 69, 203–216, https://doi.org/10.1016/S0304-4203(99)00106-1, 2000.

808 Winterwerp, J. C. and Wang, Z. B.: Man-induced regime shifts in small estuaries—I: theory, Ocean Dyn., 63,
809 1279–1292, https://doi.org/10.1007/s10236-013-0662-9, 2013.

810 WMO: Scientific Assessment of Ozone Depletion: 2018, World Meteorological Organization, Geneva,
811 Switzerland, 2018.

812 Wolfstein, K. and Kies, L.: Composition of suspended participate matter in the Elbe estuary: Implications for
813 biological and transportation processes, Dtsch. Hydrogr. Z., 51, 453–463, https://doi.org/10.1007/BF02764166,
814 1999.

815   Wrage, N., Velthof, G. L., van Beusichem, M. L., and Oenema, O.: The role of nitrifier denitrification in the
816   production of nitrous oxide, Soil Biol. Biochem., 33, 1723–1732, https://doi.org/10.1016/S0038-0717(01)00096-
817   7, 2001.

818   Yevenes, M. A., Bello, E., Sanhueza-Guevara, S., and Farías, L.: Spatial Distribution of Nitrous Oxide (N_2O) in
819   the Reloncaví Estuary–Sound and Adjacent Sea (41°–43° S), Chilean Patagonia, Estuaries Coasts, 40, 807–821,
820   https://doi.org/10.1007/s12237-016-0184-z, 2017.

821   Zander, F., Heimovaara, T., and Gebert, J.: Spatial variability of organic matter degradability in tidal Elbe
822   sediments, J. Soils Sediments, 20, 2573–2587, https://doi.org/10.1007/s11368-020-02569-4, 2020.

823   Zander, F., Groengroeft, A., Eschenbach, A., Heimovaara, T. J., and Gebert, J.: Organic matter pools in sediments
824   of the tidal Elbe river, Limnologica, 96, 125997, https://doi.org/10.1016/j.limno.2022.125997, 2022.

825   ZDM: Abfluss - Neu Darchau, edited by: Wasserstraßen- und Schifffahrtsamt Elbe, 2022.